Dissociation of Methane clathrate hydrate in Viscous fluid

Taro Kawamura, Kotaro Ohga, and Kiyoshi Higuchi

Graduate school of engineering
Hokkaido University
North 13 south 8, Kitaku, Sapporo, Hokkaido, 060-8628, Japan

Takeshi Komai, Yoshitaka Yamamoto, and Hironori Haneda

National institute of advanced industrial science and technology,
Onogawa 16-1, Tsukuba, Ibaraki, 305-8569, Japan

Introduction

Natural gas clathrate hydrates, which exist under sea ground, are recently known as big natural gas reservoir, and then expected as near future energy resources[1]. In order to recover natural gas from them commercially, in-situ dissociation of hydrate under sea ground is needed. Moreover, in case of conventional petroleum drilling (riser drilling), viscous fluids called "drilling mud" are used[2], then dissociating front of hydrate is prospected to contact with such fluids. Therefore, the information about dynamic behavior of hydrate under such condition is required. Though there are some fundamental studies about hydrate dissociation[3], practical behavior under such condition is not well understood.

In this study, dissociation kinetics of methane hydrates in viscous fluid, which have various viscosities, was investigated experimentally. Artificial pellet shaped methane hydrates were dissociated under isothermal, isobaric condition. The dissociating boundaries were directly observed, and the dissociation rates were obtained.

Experimental

Methane Hydrate Samples. The starting material was methane hydrate powder prepared by ice-gas interface method at 270K and 10MPa for about 2 days. Spectroscopic analysis of the sample material determined that more than 98% of cavities were filled with methane gas[4]. With this hydrate powder, 12-mm-o.d. and 6-mm-thickness pellets of methane hydrate were produced under pressure and temperature conditions of 30MPa and 193K, respectively. The photograph of prepared hydrate pellet is shown in **Figure 1**. Moreover, simple ice pellet was also prepared from pure ice powder to confirm the adjustment of this experimental method.

XANVIS Solution. In case of raiser drilling system, viscous fluid called "drilling mud" is used. Drilling mud usually consists of water, some salts and viscous additive material made from a kind of biopolymer. In this work, viscous additive material, XANVIS, was supplied from TELNITE CO., LTD., and its solution in distilled water was used as model mixture of drilling mud for ease. As shown in **Figure 2**, XANVIS solution has non-Newtonian flow. And it also suggests 1.0% solution had about twice viscosity to 0.4%solution at whole shear rate.

Procedure. The schematic illustration of experimental apparatus used in this work is shown in **Figure 3**. The optical cell has an inner volume of about 2ml, maximum pressure of 15MPa and is covered with sapphire window. The gas-liquid inlet, outlet and a thermo-couple are also equipped with it. Prepared pallet was set in it, and liquid cell was filled with XANVIS solution or water. Under isothermal- isobaric conditions, sample pellet was dissociated in XANVIS solution or water. The dissociating boundaries were directly observed though optical window, and the time from start of dissociation to disappearance of pellet was measured. Dissociation rate was estimated from it.

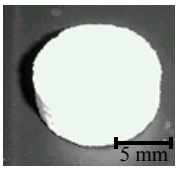

Figure 1.
Methane hydrate pellet
Height; 6 mm,
Diameter; 12 mm
Weight; 0.48-0.52 g
Porosity; 0.16-0.23

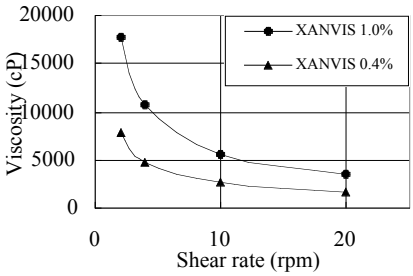

Figure 2. Viscosity of XANVIS solution. Viscosity was measured by rotary type viscometer at 279.15K.

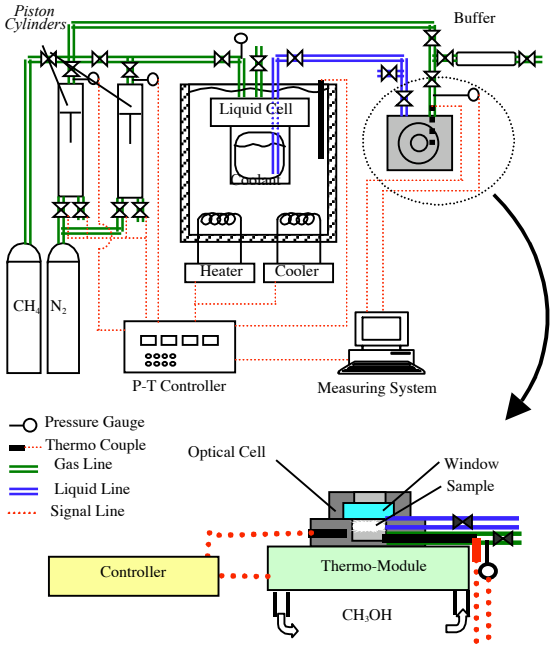

Figure 3. Schematic illustration of experimental apparatus.

Results and Discussion

Mathematical model. The mathematical model used in this work is based on simple one-dimensional thermal conduction[5]. Heat supplied from inner wall of optical cell conduct though water to hydrate (or ice) surface. Dissociation can be assumed to occur only at the surface and the surface temperature can be assumed to be its equilibrium temperature at each pressure condition. Thus, movement of the water-hydrate (or ice) interface, X, with time, t, is given by,

$$X = \lambda\sqrt{4\alpha_W \cdot t} \qquad (1)$$

$$\frac{e^{\lambda^2}}{\mathrm{erf}\lambda} = (1-\phi)\sqrt{\pi}\,\frac{\rho_H}{\rho_W}\,\frac{L_H}{C_{P,W}(T_0 - T_D)}\lambda \qquad (2)$$

Here, α_W is thermal diffusivity of water, ρ_H is density of hydrate (or ice), ρ_W is density of water, L_H is heat of dissociation of hydrate (or ice), and $C_{P,W}$ is heat capacity of water. The measured porosity of

hydrate □ was about 0.195. T_0 is the experimental temperature, and T_D, the hydrate (or ice) dissociation temperature, is set by the applied pressure. The adjustments of this model to experimental results, which were obtained from ice-water (XANVIS 0%) system, hydrate-water (XANVIS 0%) system, and hydrate-XANVIS solution system, were evaluated below.

Dissociation rate of Ice-Water system. Time required for vanish the ice pellet at each temperature is shown in **Figure 4**. Experimental result shows exponential trend; the time become long, as dissociating condition become close to equilibrium (273.15K, 0.1MPa). Vanishing time obtained from experiment and calculated value with eq. (1) show same trend and each value show reasonable agreement in error by 1.3min.

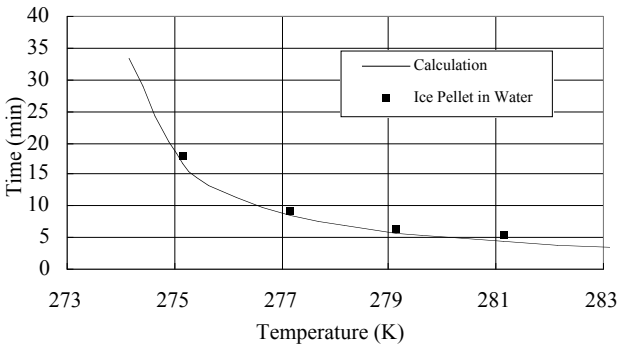

Figure 4. Time required for vanish the ice pellet at each temperature under atmospheric condition.

Dissociation rate of Hydrate-XANVIS Solution system. **Figure 5** shows time required for vanish the hydrate pellet in each pressure-temperature-viscous condition. Each symbol represents experimental value. Lines represent obtained value from model calculation of hydrate-water (XANVIS 0%) system. Each value shows same exponential trend; the time become long, as dissociating condition become close to its equilibrium condition. On hydrate-water system, experimental results and calculated value show reasonable agreement at relatively low-pressure. However, experimental results show larger value than calculation, as the condition become cloth to equilibrium. At higher XANVIS concentration, obtained vanishing time took large value. This trend is shown at whole pressure condition.

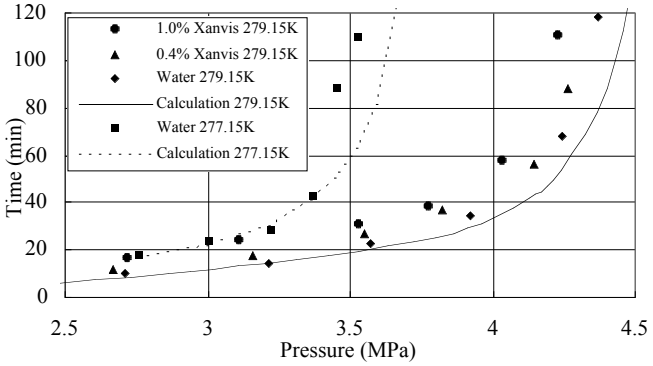

Figure 5. Time required for vanish the hydrate pellet at each condition.

Observed Dissociating boundary. Dissociating hydrate surfaces in three different viscous fluids are shown in **Figure 6**. Dissociating surface of ice is appended for comparison. During dissociation, though almost no bubble were shown on ice surface (see **Fig.6 a**), whole surface of each hydrate was covered with methane bubbles, which were generated by hydrate dissociation. In case of hydrate-water system (XANVIS 0%), small bubbles moved away from hydrate surfaces rapidly (see **Fig.6 b**). For 0.4% XANVIS solution, generating bubbles moved through the fluid slowly, then small bubbles combined each other to become relatively large one (see **Fig.6 c**). In case of 1.0%, bubbles moved very slowly on hydrate surfaces, and its sizes became large compared with former two cases (see **Fig.6 d**).

Since existence of bubbles causes thermal resistance, vanishing time is considered to become late. On the contrary, moving bubbles draw convection heat transfer. Then, it seems to accelerate the dissociation. On the other hand, influences of bubbles are neglected in the mathematical model. Therefore, it is considered that influence of bubbles is one of primary factor of misfit of calculated value to experimental results in hydrate-water system. At higher XANVIS concentration, it was also considered that the trend; vanishing time shift to long as concentration, was caused by the bubbles. Of course, the influence of heat capacity change of solution needs to be investigated.

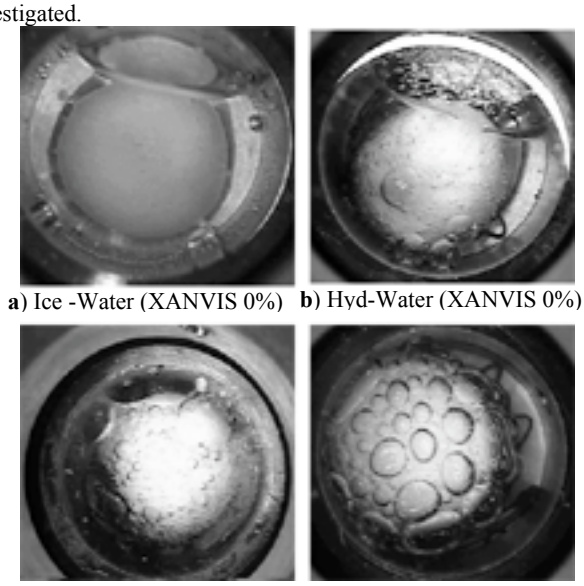

a) Ice -Water (XANVIS 0%) **b**) Hyd-Water (XANVIS 0%)

c) Hyd-XANVIS 0.4% **d**) Hyd- XANVIS 1.0%

Figure 6. Snapshots of dissociating pellet surfaces. Ice pallet was at 275.15K, hydrate pellets were at 279.15K, 3.8MPa respectively.

Conclusion

Experimental results, which were obtained from simple ice-water system, fitted well to model calculation. In case of hydrate-water system, it was considered that influence of bubbles is one of primary factor of the misfit of them. The bubble influence was also seemed to affect on dissociation in hydrate-XANVIS solution system. We attempt to construct more practical model, considering to the influence of bubbles and so on.

References

1. Sloan, E. D., Clathrate hydrates of natural gas, Marcel Dekker, New York, **1998**
2. Berthezene, N., de Hemptinne, J. C., Audibert, A., Argillier, J. F., J. Petro. Sci. Eng., **1999**, 23, 71-81
3. Clarke, M., Bishnoi, P. R., Chem. Eng. Sci., **2000**, 55, 4869-4883
4. Hirai, H., Kondo, T., Hasegawa, M., Yagi, T., Yamamoto, Y., Komai, T., Nagashima, K., Sakashita, M., Fujihisa, H., & Aoki, K., J. Phys. Chem. B, **2000**, 104, 1429-1433
5. Keikar, S. K., Selim, M. S., Sloan. E. D., Fluid Phase Equilibria, **1998**, 150, 371-382

EFFECT OF POROUS MEDIA ON THE CONDITIONS OF DICHLORODIFLUOROMETHANE HYDRATE DISSOCIATION

E. A. Bondarev, A. Z. Savvin

Institute of Oil and Gas Problems
October Str., 1
677891 Yakutsk, Russia

Introduction

Study of gas hydrates in porous media became a matter of interest for the following reasons. Practice of developing natural gas fields, in the regions of permafrost particularly, has revealed the probability of hydrate formation in the bottom hole zone that reduces the well productivity. Also, thermodynamic conditions in the Earth's crust and in the World Ocean sediments may be such that they will favor the formation of large accumulations of hydrocarbon gases in a hydrate form.

Among the factors influencing the equilibrium conditions of hydrate formation (temperature and pressure) in porous media, aside from gas composition and pore water salinity, one can point out mineralogical and granulometric composition and moisture content of a medium. Numerous investigations have been carried out in order to determine the equilibrium conditions of hydrate formation in the absence of a porous medium. Their detailed review is presented in [1]. However, the analysis of the few works where the effect of rock properties on the phase equilibrium of hydrates has been studied reveals the absence of reliable experimental data, the available ones contradicting each other in some cases [2 - 6]. For example, it was stated in one of the first works that hydrate formation temperature in the sand rocks is 2-5 K lower then that for a pure hydrate (in the absence of a porous medium) [2]. The experiments with the tetrahydrofuran hydrate have shown that the porous medium consisting of sand and glass spheres with the diameter of 1.0 and 0.1 mm does not affect its thermophysical properties as well as its melting temperature [3]. A considerable shift of the phase equilibrium curve toward the lower pressure (about 50%) is observed during hydrate formation in water bentonite suspension [4]. On the other hand, a slight excess of the equilibrium pressure by 78 kPa in comparison with a pure hydrate at the same temperature has been observed during the experiments on methane hydrate formation and dissociation in natural water-saturated cores [5]. The experiments on hydrate formation in the clay rock have shown that the water layer the most tightly bound to the surface of particles has not been involved in hydrate formation [6]. Pressure and temperature of freon-12 and propane hydrate dissociation in porous media have been determined during the experiments on moisture migration during hydrate formation [7]. It has been established that dissociation pressure for the propane hydrate in the sand with the grain fraction of 0.1-0.25 mm and moisture of 20% is 10-20 kPa higher than that for a pure hydrate.
The aim of the present study is to investigate the effect of a type and moisture content of the porous medium on the phase equilibrium in the system hydrate – gas – water.

Experiment

Temperature of hydrate dissociation at a given pressure has been determined by the differential thermal analysis with the help of the laboratory device shown in Figure 1. In the duralumin heat unit 1 there are two symmetric cells 2, 3 in the form of a cylinder where polytetrafluoroethylene ampules with the primary standard and the sample under the study are placed. The heat unit is inserted in a steel high-pressure chamber 4 where gas is injected through the input system consisting of a container 9 with a gas, valves 10, 11 and high pressure pipes. Pressure in the chamber is measured with the manometer 13. To measure temperature in the sample and temperature difference between the standard and the sample we use the combined thermocouple consisting of two differential copper-constantan thermocouples 7, 8, cold junctions of which are placed in the Dewar vessel 6 at 273.15 K. Thermocouple readings are amplified (amplifiers 14, 15) and then, by means of the matching facilities, are transferred to the input of the multichannel potentiometer 16. Instrumental error of temperature measurements is determined by the error of the thermocouple graduation and that of thermoEMF (electromotive force) measurements and does not exceed $\pm$ 0.1K. Pressure in the chamber is measured by manometers, the error being less than $\pm$ 4 kPa.

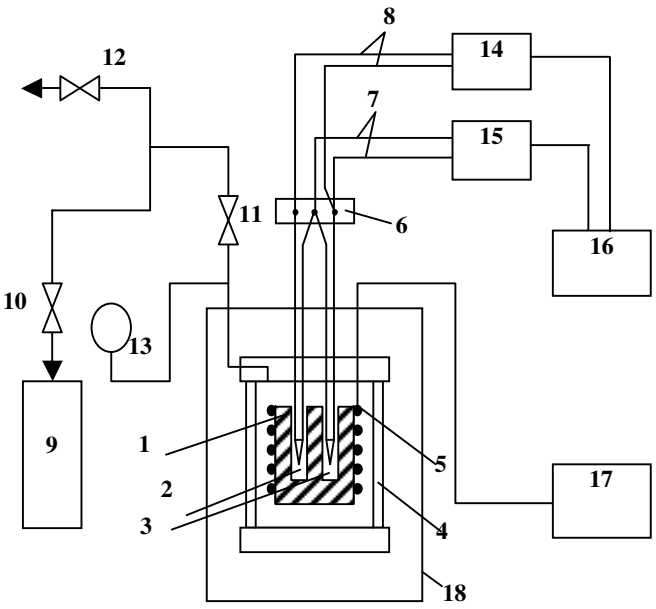

Figure 1. Sheme of the experimental device

At this stage of the study we used, as a hydrate former, the dichlorodifluoromethane CCl_2F_2 (freon-12) with the volume content of 99.5 %. Freon-12 forms the hydrate of Structure II. The porous medium is the quartz and river sand with the fraction of 0.15-0.25 mm, sand and clay mixture, obtained from the natural rock by sieving through the 0.08 mm sieve, and bentonite. According to the granulometric classification of dispersion media [8,9] the clay and sand mixture contains clay (<0.001 mm) and dust (0.001-0.05 mm) particles and fine-grained sand (0.05-0.08 mm). Bentonite is classified as highly disperse clay and consists of particles of <0.001mm size (85-90%). To remove water-soluble salts the samples are washed with hot distilled water followed by the analysis of the water extract in order to detect corresponding ions. Hygroscopic moisture of the samples is obtained by sorption during their keeping desiccators with pure water and solutions of sulfuric acid or kalium sulfate at 293 K within a month. The above method of moisture setting provides the most uniform distribution of water through the rock volume. Moisture content of the samples exceeding the maximum hygroscopic one is obtained by the contact method followed by their keeping in the in the desiccators with the distilled water within one or two weeks. Maximum hygroscopic moisture content is considered as

water quantity which rock absorbs from the environment at a relative moisture content φ =1.0. Moisture content of the samples (i.e. percentage relation of water mass in the rock sample to the mass of the dry sample) is measured by weighing. Mass of the dry sample is determined after its drying at 378 K. to a constant value.

The experiments have been performed in the following way. The heat unit with a sample of a porous medium at a given moisture content and the standard are placed into the high-pressure chamber. Then, with the help of the pump through the valve 12 vacuum is created in the chamber after that it has been filled with the gas under pressure of 0.4-0.5 MPa. The chamber is slowly cooled in the thermostat 18 to 276 K, at which freon is in liquid state. Hydrate formation is initiated by the evaporation of liquid freon. As a result, the pressure of the gaseous freon exceeding that of hydrate dissociation at the given temperature is set in the working chamber. After two or three days the standard and the sample are subjected to heating so that the linear temperature growth occurs. In our experiments the rate of heating has been about 10^{-3} K/s. Hydrate dissociation is revealed by a sharp peak-like deviation of the curve of the temperature difference between the sample and the standard. It is known that in this case the sample temperature at the same moment is the temperature of the phase transition [10,11].

Results and discussion

The data obtained for the temperature of the CCl_2F_2 hydrate dissociation are presented in Tables 1, 2. The experimental data show that at the same pressure the dissociation temperatures of the pure hydrate and the hydrate in the quartz and river sand are equal within the limits of a measurement error at moisture content of the sand being higher than that of the maximum hygroscopic one (W_{mg} = 0.96 %). Moisture content interval under study is 0.96-20.0 %. At W_{mg} = 0.96 % there is the drop of the temperature of hydrate dissociation in sand to $\Delta T = T_0 - T$ = 0.8 K (T_0 =279.4 K is the temperature of pure hydrate dissociation at P_0 =123 kPa).

Table 1. Conditions of CCl_2F_2 hydrate dissociation in the sand and clay and sand mixture

P, kPa	*T*, K (pure hydrate)	*T*, K (sand, *W*=3.2 %)	*T*, K (clay and sand mixture at moisture content *W*, %)		
			29.8	11.2	8.3
105	278.7	278.7	278.6	277.8	-
123	279.4	279.4	279.4	278.6	277.5
184	280.9	281.0	-	280.1	278.9
255	282.4	282.5	282.4	281.6	280.8

Similar dependence between the dissociation temperature and moisture content of the rock is observed for the hydrate formed from the pore water contained in the clay and sand mixture and bentonite. At moisture content $W > W_{mg}$=12.2 % for the clay and sand mixture and $W > W_{mg}$=43.3 % for bentonite dissociation temperatures of the pure hydrate and the hydrate formed from pore water are equal within the limits of a measurement error. At moisture content being less than that of the maximum hygroscopic one temperature drop of hydrate dissociation occurs, the lower the moisture content, the lower the temperature. If the dissociation temperature in the clay and sand mixture drops approximately by 2 K at *W*=8.3%, that in such a highly dispersion medium as bentonite drops by 2 K at *W*=39.8%.

Statistical processing of the experimental data shows that the total error at measuring the dissociation temperature, represented by a confidence limit, is not more than $\pm$ 0.3 K at probability being equal to 0.95.

Table 2. Conditions of CCl_2F_2 hydrate dissociation in bentonite

P, kPa	*T*, K at moisture content of the rock *W*, %		
	49.4	39.8	34.7
105	278.7	276.8	275.7
123	279.4	277.6	276.3
184	280.8	279.4	278.1
255	282.4	280.8	279.9

There is a certain relation between the maximum hygroscopic moisture content and the specific surface of the porous media under study, i.e. the larger the specific surface, the higher W_{mg}. Thus, W_{mg} may serve as some peculiar characteristics of the rock dispersion.

In the region of the hygroscopic moisture content of porous media water occupies mesopores due to the capillary condensation, i.e. at the pressure of the water vapor over the concave meniscus which is less than that of the saturated vapor over the flat surface. The reduced pressure of water vapor in such capillaries causes a temperature drop of hydrate dissociation in the porous medium as compared with the dissociation temperature of the pure hydrate. Thus, porous media at moisture content being less than that of the maximum hygroscopic one affect the phase equilibrium in the system hydrate – gas – water. The above effect manifests itself by a shift of the phase equilibrium curve in the direction of lower temperatures. The lower moisture content of the porous medium, the lower hydrate dissociation temperature.

References

1. Byk S.Sh., Fomina V.I. Gas hydrates. M.: Khimiya, 1980.
2. Makogon Yu.F. Hydrates of natural gases. M.: Nedra, 1974.
3. Rueff R.M., Sloan E.D Ind. Eng. Chem. Process Des. Dev., 1985, v. 24, No. 3, p. 882-885.
4. Cha S.B., Ouar H., Wildeman T.R., Sloan E.D. J. Chem Phys., 1988, v. 92, No. 23, p. 6492-6494.
5. Yousif M.H., Sloan E.D. SPE Reservoir Engineering, 1991, No. 12, p. 452-458.
6. Yakushev V.S. In: Natural and Technogenic Gas Hydrates. M.: VNIIGAS, 1990, p. 174-187.
7. Melnikov V.P., Nesterov A.N. Ground Freezing 97, Knutsson (ed), Balkema, Rotterdam, 1997, p. 391-395.
8. Efimov S.S. Moisture of hygroscopic materials. Novosibirsk: Nauka, 1986.
9. Soil Science/Edited by Sergeiev E.M. M.: Moscow State Univ. Publ., 1983.
10. Berg L.G. Introduction to thermography. M.: Nauka, 1969.
11. Piloyan G.O. Introduction to the theory of thermal analysis. M.: Nauka, 1964.

A Field Oriented Natural Gas Hydrate Research Project for The Alaska North Slope – Resource Evaluation And Possible Testing

Keith Millheim and Jonathan Kwan

Anadarko Petroleum Corporation
17001 Northchase Dr. Houston, TX 77060

Williams Maurer

Maurer Technology Inc.
2916 West T.C. Jester, Houston, TX 77018

Abstract

For years natural gas hydrates have portended potential multi-trillion cubic feet of primarily methane reserves both onshore and offshore. Recently, two major events have moved the hydrate curiosity to serious hydrate interest: (1) The perceived ensuing shortage of accessible cost effective energy for North America and other countries like Japan, and (2) The stimulus by the National Energy Technology Laboratory/US Department of Energy (NETL/DOE) hydrate program to fast forward hydrate technology.

Anadarko Petroleum Corp. along with Mauerer Technology and Noble Engineering are participating in the recent Alaska hydrate research program sponsored by NETL/DOE. This unique field oriented research project will apply known oil and gas technology with modification to recognize and access North Slope hydrate gas accumulations with a further plan to attempt long term well production testing of the wells that will be drilled during the project. The research program incorporated some of the unique approaches to the coring, core retrievable core assessment, well bore evaluation, including the various testing scenarios. On-site laboratory testing will be done when appropriated to understand the time function on some of the physical properties. Thermodynamics and kinetics data will be obtained from off-site measurements

Introduction

Gas hydrates occur naturally in permafrost and deep marine environments around the globe. It is estimated that methane in gas hydrates worldwide is more than 10^{13} tons of methane-carbon [1]. This quantity is equivalent to ~2.10^{16} cubic meters of methane gas, or about twice as much as all other fossil fuels, taken together. and about 370 times as much as all of the natural gas ever likely to be produced from conventional sources in North America [2]. Potentially, this resource could be the backbone for the world's energy sector during the 21st century.

Background

Several major factors have so far prevented the commercialization of gas hydrates to produce clean burning, environmentally friendly fuel. These factors are:

- Remoteness of the hydrate resources from major natural gas markets, except in several cases (offshore the East Coast of the United States, offshore Japan, offshore India, in the Black Sea, and offshore Australia);
- Insufficient knowledge about the in-situ properties of gas hydrates;
- Absence of economical and proven technology for the production of natural gas from gas hydrates;

Remoteness of the resource - no more. Even gas hydrates have been recovered in at least 90 locations in marine environments globally and in many cases in permafrost conditions onshore, these sites are often situated far from the major natural gas markets. For example, it would take a 5,000 km pipeline to bring gas from Alaska to the continental United States, and even if gas hydrates were to be successfully developed, the cost of transportation may be prohibitive. However, the situation changed when the N. America gas market get tight and several plans on gas pipeline from Alaska and Canada to the United States have been under intensive debate. The known gas resource on the North Slope, 35 trillion cubic feet (Tcf) are the energy equivalent to six billion barrels of oil, half the oil reserves in Prudhoe Bay. Up to 100 Tcf of gas could eventually be developed on the slope. This is not including the potential hydrate deposit under the permafrost and offshore Beaufort Sea. Due to its shallow depositional environment, hydrate can be a low cost energy source.

To evaluate the costs and benefits of bringing natural gas from gas hydrates to markets, the knowledge of the hydrate physical properties and the technologies for their production would first have to be developed and tested. Significant laboratory knowledge in gas hydrates is available, but the hands-on field experiences are few.

Insufficient knowledge – Improving. While it is easy to create gas hydrates in laboratory experiments, there are few hydrate samples (both in pressurized and non-pressurized containers) from natural deposits. In 1998, the completion of a 1150 meters hydrate test well Mallik 2L-38 in the MacKenzie Delta, NWT, Canada have made significant improvement in the knowledge base of naturally occurring hydrates [3]. The scientific project focused on geophysical measurements with limited hydrate coring. Approximately 37 meters of hydrate cores were recovered with very scarce publications on their test results. Such research requires the ability to recover, transport, prepare and analyze samples under controlled conditions identical to the ones in-situ. Currently there is no comprehensive program of this kind. The insufficient knowledge about gas hydrates properties in natural environments is a serious handicap for the development of technologies to produce methane from gas hydrates.

Absence of proven technologies – adopted and modified from existing industry. The Mallik well have employed several new and innovative coring designs and procedures with reasonable but limited success. There are several known technologies to extract natural gas from gas hydrates, mostly based on the use of techniques leading to the decomposition of the hydrates in-situ and the subsequent production of the gas by conventional or adapted gas wells. For example, gas hydrates decompose when the pressure and temperature are beyond certain limits, or when inhibitors are injected, and the gas is released and can be produced by wells.

There is one known case where natural gas has been commercially produced from gas hydrates for a sustained period of time. In permafrost onshore North Siberia in Russia, inhibitors were injected to cause the decomposition of the gas hydrates, and the released gas was produced at the Messoyakha gas field. Production was discontinued when it was judged uneconomic. In recent publications, the claim that the produced gas did actually originate from the gas hydrates, and not from free gas trapped under the gas hydrates in the Messoyakha field, has been disputed. It is inevitable that the hydrate production technology will be derived from the well-developed oil and gas practices. Under the contract terms with NETL/DOE, this research program will focus on the identification of the hydrate area, coring operation, test hydrate properties and monitor the wellbore. Production is only a secondary objective.

Site Selection and Permitting

Site selection is based on Anadarko proprietary seismic data and available public information from various well logs and temperature logs. The current selections of possible site are a balance between easy access to roads, potential hydrate thickness and safe operation conditions. Due to environmental concerns and regulatory stipulations in the Alaska Coastal and Foothill areas; the permitting processes are very lengthy. Other than the permitting requirements from the Federal and State agencies, local authorities, native and various citizen groups have to be informed of all drilling activities. The drilling season in the Arctic is only opened for the few months in winter. With all the logistic of mobilizing the equipment, the actual drilling window is very limited. Water and gravel usage to build ice road and site preparation is under rigorous control.

Drilling and Coring

Three straight holes will be drill and core from the permafrost through the hydrate zone. A small-footprint mining/coring rig will be used in the drilling and coring operation to minimize the environmental impacts in the tundra. Selection of coring equipment is underway with carefully planned operation procedures that meet all environmental and safety requirements. Fluid chilling will be used if the operational time frame will destabilize the hydrate core. Other than the thermodynamic properties, the kinetics reaction during coring of the hydrate is critical. The time-dependent hydrate freeze and thaw cycle in the presence of coring fluid may provide a self-preservation mechanism. Several drilling/coring fluids will be tested in the laboratory for its compatibility with the hydrate (laboratory simulated). The stringent requirement of the coring fluid will ensure and maximize core recovery. The data from laboratory measurement will feed into a computer wellbore simulator to ensure a safe operation. All equipment will be tested prior moving on location. Mud logging will be used to identify the hydrate stabilization zone. Gas and fluid compositions are good indicators.

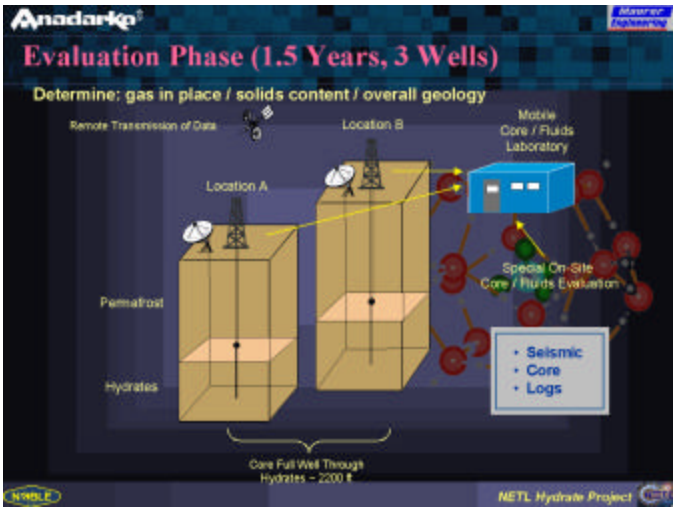

Fig. 1 Hydrate Evaluation Phase

Core Preservation and Laboratory Testing

The stability of gas hydrate is dependent on pressure, temperature and the solubility of gas as a function of pressure and temperature in the system. Understanding of the thermodynamic data of methane and other gas hydrates is very important from the view-point of preserving cores and exploiting natural gas production from hydrate wells. The hydrate handling experiences from various National Laboratories and the USGS indicated the stability of hydrate is more susceptible to changes in temperature than pressure during the time of coring and core preservation at the well site. During the coring operation, recovered cores will be kept at a specific (low) temperature to preserve its original properties by means of an insulated core holder. For longer term core storage, the hydrate cores will be kept in pressure core storage barrels and under proper temperature. Appropriate tests on-site and off-site using known laboratory techniques.

Geophysical and Petrophysical Properties. While the centerpiece of laboratory testing has been to understand the seismic response of hydrate and fluids and seismic relationships with petrophysical parameters, data can also be generated for reservoir quality evaluation, seismic characterization, petrophysical evaluation, and hydrate reservoir mechanical/chemical stability evaluation. The laboratory is highly automated with high sample throughput capability.

Thermal Properties. The basic properties important for understanding the thermal state of the hydrate reservoir are temperature, thermal conductivity and thermal diffusivity [4]. Time Temperature Transformation (TTT) profiles can be constructed from isothermal Differential Scanning Calorimetry (DSC) data. It will provide information about the complex nucleation and growth mechanism. This simple technique can be used to screen the efficiency of different chemical inhibitors. Results can provide heat flow Vs reference temperatures data with heats of fusion and crystallization resolving Ice and Hydrates distinctly

Table 1. Hydrate Core Characterization Measurements

Seismic	**Compression & Shear Velocities @various *P & T***
	Elastic Anisotropy
Petro -	**Porosity & Permeability @ various *P &T* (NMR)**
Physical	**Bulk and Grain Density**
	X-ray & FTIR Mineralogy
	Laser Particle Size Analysis
Engineering	**Compressive strength**
	Young's Modulus
Thermal	**Conductivity & Diffusivity**
	Heat of fusion
Chemical	**Carbon Isotope**
	Fluid & Gas Composition

Open Hole Logging and Completion

The basic sonic, SP and Gamma logs will be run after the cores are recovered. NMR is rather unique to apply in the investigation of hydrates. There are only two companies that can provide the NMR tool. Currently, only one will service the Alaska North Slope. The electronic logs will be analyzed in conjunction with the laboratory core testing results, the mud log data and seismic data. After the logs are done, these wells will be equipped with temperature strips and downhole pressure gauges for temperature and pressure profile monitoring. Various precautions will be observed to log the borehole temperature if fluids are accumulated inside the wellbore. Time will allow to let the wellbore to get in equilibrium with the surrounding formation. Simple techniques such as thermal stimulation will be applied to the wellbore to observe its respond.

Conclusions

The objective of this research project is to develop technologies that can be used for the continuation of a long-term product test at one or more hydrate sites in the arctic environment, and upon the confirmation of its viability, the immediate commercialization of the technology. The project is also expected to assess the natural gas reserves of gas hydrates resources in the arctic and the elaboration of recommendations to facilitate the commercialization of a vast, environmentally friendly source of fossil energy in Alaska and worldwide.

Acknowledgement. The authors like to thank the National Energy Technology Laboratory (NETL), Department of Energy for their generous support with contract # DE-PS26-01NT40869-2, and the management support of Anadarko Petroleum Corporation, Maurer Technology Inc., a unit of Noble Drilling Company.

References

(1) Kvenvolden, K.A., Ginsburg, G.D. and Soloviev, V.A. – *Geo-Marine Letters.*, **1993**, *13*, pp.32-40.

(2) Kvenvolden, K.A., *Natural Gas Hydrate: Introduction and History of Discovery* Chapter 2 in *Natural Gas Hydrate in Oceanic and Permafrost Environments*, Max, M.D., Ed.; Kluwer Academic Publishers, **2000**; pp. 9-16.

(3) Dallimore, S.R., Uchida, T. and Collett, T.S., *GSC Bulletin 544 Scientific Results from JAPEX/JNOC/GSC Mallik 2L-38 Gas Hydrate Research Well, Mackenzie Delta, Northwest Territories, Canada*, **1999**.

(4) Ruppel, C., *Thermal State of the Gas Hydrate Reservoir*, in *Natural Gas Hydrate, Chapter4 in Oceanic and Permafrost Environments*, Max, M.D., Ed.; Kluwer Academic Publishers, **2000**; pp.29-42

Gas Hydrate Crystal Growth and Decomposition

C.A. Koh*[a] , S.C. Nyburg[a], A.K. Soper[b], S. Parker[b], R.E. Westacott[c], J. Creek[d], S. Subramanian[d]

[a]*King's College London, Department of Chemistry, Strand, London WC2R 2LS, U.K.*
[b]*ISIS Facility, Rutherford Appleton Laboratory, Chilton, Didcot, Oxon., OX11 0QX, U.K.*
[c]*Heriot-Watt University, Department of Mechanical & Chemical Engineering, Edinburgh, EH14 4AS, U.K.*
[d]*Chevron Petroleum Technology, Houston, TX 77082, U.S.A.*

The formation and decomposition of gas hydrates are of both fundamental and industrial importance.[1-3] Further insight into these processes is needed in order to control hydrate crystallisation in gas/oil pipelines, or for the extraction of methane hydrate from marine sediments.

Crystal growth[4] and decomposition processes have been examined for methane hydrate using *in situ* neutron diffraction measurements. The methane hydrate samples were synthesized by charging a high pressure variable temperature TiZr cell with D_2O and pressurising with CH_4 and CD_4. The liquid in the reaction cell was cooled using a recirculating glycol bath. Fine temperature control of the cell was achieved using electrical heating, with thermocouples placed within the copper cooling jackets at the top and bottom of the cell. The D_2O/methane mixture was allowed to equilibrate at around 18°C and 14.5 MPa while agitating the fluid within the cell vigorously to ensure effective interfacial mixing. The temperature was lowered in stages such that the system was driven towards methane hydrate formation. On complete hydrate conversion of the liquid within the neutron beam (indicated by the absence of any diffuse scattering), the temperature was subsequently increased in stages until the methane hydrate was completely decomposed. At this stage, the temperature was well outside the hydrate formation region and the neutron diffraction pattern gave no indication of Bragg reflections due to hydrate crystals (see Figure 1).

These neutron diffraction measurements were coupled with simultaneous gas consumption measurements, which were performed throughout the duration of the experiments. This is the first molecular-level study of methane hydrate decomposition and is expected to provide insight into the structure of the liquid phase immediately after dissociation of the hydrate crystal lattice.

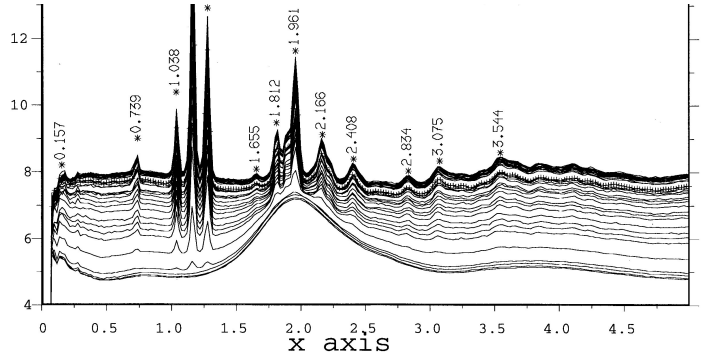

Figure 1. Neutron scattering cross-section data during methane hydrate decomposition (CH_4/D_2O).

The phonon density of states of methane hydrate and THF hydrate (a model sII hydrate) has also been measured using inelastic neutron scattering. Methane hydrate samples were prepared from fine particles of H_2O and D_2O ice pressurised with methane gas. The effect of a thermodynamic inhibitor, methanol, on the structure and dynamics of these systems has been investigated. Important structural information on methane hydrate and carbon dioxide hydrate has also been extracted from *in situ* neutron and X-ray diffraction data.

References

(1) Sloan, E.D. *Clathrate Hydrates of Natural Gases,* 2nd Edition, 1997, Marcel Dekker, N.Y.
(2) Englezos, P. *Ind. Eng. Chem. Res.,* **1993**, 32, 1251.
(3) Koh, C.A.; Westacott, R.E.; Zhang, W.; Hirachand, K.; Creek, J.L.; Soper, A.K. *Fluid Phase Equilibria*, **2001**, 4848, 1.
(4) Koh, C.A.; Wisbey, R.P.; Wu, X.; Westacott, R.E.; Soper, A.K. *J. Chem. Phys*. **2000**, 113, 6390.

KINETIC INHIBITION OF METHANE HYDRATE BY POLYMERS

Ugur Karaaslan and Mahmut Parlaktuna

Department of Petroleum and Natural Gas Engineering,
Middle East Technical University, 06531 Ankara, Turkey

Introduction

Gas hydrates are ice-like crystalline compounds that are formed by the combination of water molecules with gas molecules under suitable conditions of pressure and temperature. Water molecules form a lattice structure with cavities that are occupied by gas molecules. There is no chemical union between the water and gas molecules. The water molecules that form the lattice are strongly hydrogen bonded with each other and the gas molecule interacts with water molecules through van der Waals type dispersion force[1].

In the industry, there is an increasing tendency to exploit hydrocarbon reserves at increasing depths in the oceans and with increasing distances for pipeline transportation in both horizontal and vertical directions. Due to this extended exposure of the water-containing unprocessed hydrocarbon fluid to low temperatures and high pressures, the handling of the hydrate problems in such transport lines has become a more integral part of the petroleum industry. Since large percentages of alcohol have to be added, an economic incitement towards more effective inhibitors has evolved. The focus over the last few years has been directed towards slowing down the process of hydrate formation, kinetic inhibition. In this context studying the fundamental kinetics of hydrate formation is importance.

Hydrate inhibitors are classified into three groups: Thermodynamic inhibitors, kinetic inhibitors and anti-agglomerates. Thermodynamic inhibitors are used at high concentrations (10-60 wt %), kinetic inhibitors and anti-agglomerates are added at low concentrations (<1 wt %). The latter do not affect the thermodynamics of hydrate formation, however, they do delay hydrate nucleation and/or crystal growth. Anti-agglomerates prevent the agglomeration of hydrates so that all the hydrate crystals are transportable in a pipeline. Both kinetic inhibitors and anti-agglomerates are usually polymers with surfactant properties[2].

The inhibition mechanism of polymers and surfactants is proposed as follows: Active molecules are found to adsorb strongly to the surface of a propagating hydrate crystal or pre-nuclear hydrate like clusters. In this process, they change the energy of the surface of hydrate crystal or cluster and so change its growth characteristics[3]. The poly(N-vinyl pyrrolidone) (PVP), poly(N-vinylcaprolactam) (PVCap), poly(N-methyl-N-vinylacetamide) (VIMA), poly(N-vinylvalerolactam) (PVVam) and poly(acryoylpyrrolidine) (PAPYD) are some examples of known and patented inhibitors[4].

In this study hydrate inhibition potential of different polymers have been tested in a high-pressure apparatus at high pressures and low temperatures with varying polymer concentration. A known hydrate inhibitor, poly(N-vinylpyrrolidone) (PVP) and a water soluble thermoplastic polymer (PEO) were determined the best kinetic inhibitors among them.

Experimental

Set-Up. A high-pressure system, whose schematic diagram is given in **Figure 1**, is used to carry out hydrate formation tests. A cylindrical high-pressure reactor with dimensions of 3.4 cm in diameter, 15 cm in length is the main piece of experimental set-up. Its total available volume is 142 cm^3 including connections. It is made of brass and tested up to 1200 psi. The high-pressure cell is placed into a constant temperature bath made by plexiglass allowing the observation of the system easily. A temperature controller and a refrigerated chiller are immersed into the water bath to provide temperature control during tests. A thermocouple (with an accuracy of ±0.2 °C) and a pressure transducer (with an accuracy of ±1 psig) are connected into the high-pressure cell to measure cell temperature and pressure. They are connected to a data-logger and a personal computer to record the temperature and pressure as functions of time. A motor at the outside of the bath is attached to the cell to provide rocking, and a glass marble is placed into the cell to stir and agitate the liquid inside. The speed of the rocking system was kept at 30 RPM; temperature and pressure are recorded every 10 seconds throughout this study. Methane gas that has 99.5 % purity was used as hydrate former gas. Aqueous polymer solutions were prepared in pure water.

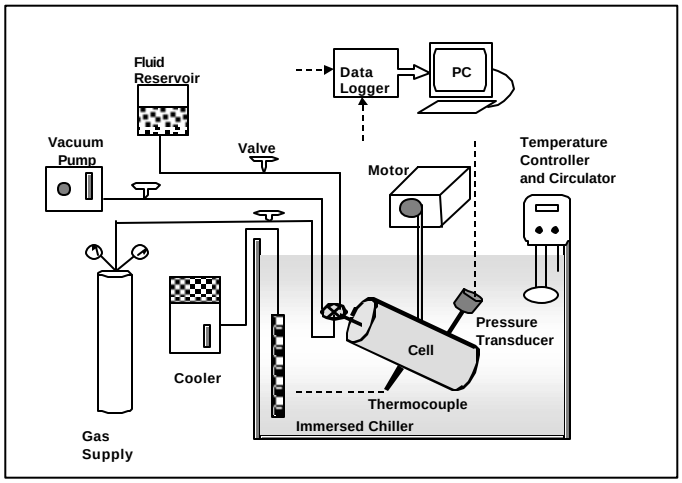

Figure 1. Schematic representation of experimental set-up.

Procedure. After making the necessary connections (gas, water, and vacuum lines, thermocouple and pressure transducer connections) to the high-pressure cell, the system is evacuated. Then, aqueous phase is injected into cell and the cell is pressurised by methane gas. After reaching in equilibrium at initial pressure and temperature conditions (**Table 1**), the system is cooled down to hydrate formation temperature without rocking meanwhile data collection is started. Rocking process is started to agitate the solution in the cell to initiate hydrate formation at predetermined hydrate formation temperature. At that point, the cell pressure already decreased from 700 psig to 662 psig due to cooling and dissolution of methane gas at low temperature. Details of the experimental procedure can be found from Karaaslan[5].

Table 1 Experimental Conditions

Test No	weight (%)	$T_{initial}$ (°C)	$P_{initial}$ (psig)	$T_{rocking}$ (°C)	$P_{rocking}$ (psig)

T-1	pure water	15	700	3	662
T-2	0.010 PVP	15	700	3	662
T-3	0.100 PVP	15	700	3	662
T-4	0.500 PVP	15	700	3	662
T-5	1.000 PVP	15	700	3	662
T-6	0.010 PEO	15	700	3	662
T-7	0.025 PEO	15	700	3	662
T-8	0.050 PEO	15	700	3	662
T-9	0.100 PEO	15	700	3	662
T-10	1.000 PEO	15	700	3	662

Results and Discussion

Kinetics. Rocking of cell inside hydrate formation region triggers hydrate formation and a decrease in pressure is observed. Pressure-temperature data of each test through real gas law are used to calculate the moles of remaining free gas in the cell during methane hydrate formation. Moles of free gas in the high-pressure cell as function of time for pure water (0.00 %), PVP and PEO solutions are given in **Figure 2** and **Figure 3,** respectively. As it is seen from the Figure 2, number of moles of free gas decreases with time for pure water due to hydrate formation. On the other hand, there is almost no change in moles of free gas when 0.1, 0.5 and 1 weight % of PVP solutions are used as hydrate forming media. Although 0.01 weight % PVP solution retarded the hydrate formation for a period of 40-45 minutes, after that time the hydrate formation accelerated, indicating that the inhibitor lost its efficiency.

As seen from Figure 3, the tests with PEO solutions show the same behavior as PVP tests. It is obvious from figure that PEO is an effective inhibitor as compared to the pure water experiment. Free gas consumption is less for all concentrations than observed with pure water (0 weight %). The highest inhibitor efficiency was determined at and higher concentrations of 0.1 weight % PEO solution. Free gas versus time plots also show that hydrate inhibition efficiency of PEO increases with increasing concentration.

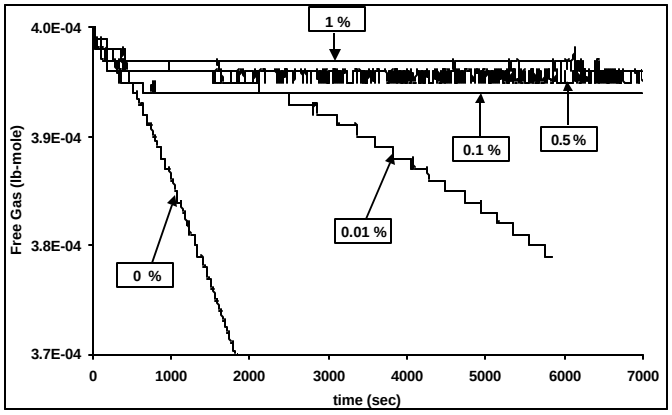

Figure 2. Methane hydrate formation with 0, 0.01, 0.1, 0.5 and 1 weight % PVP solutions.

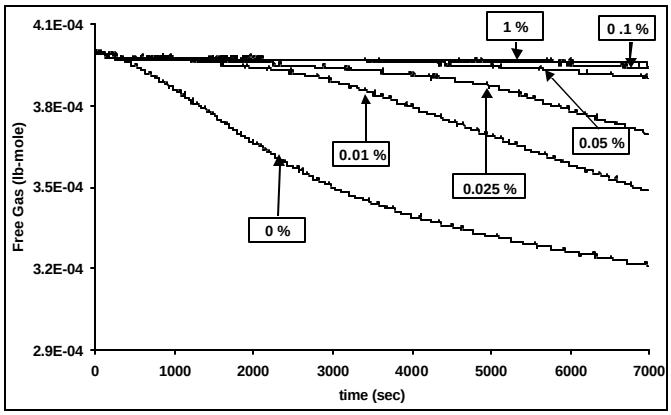

Figure 3. Methane hydrate formation in 0, 0.01, 0.025, 0.05, 0.1 and 1% PEO solutions.

Hydrate Formation Rates. Rate of change of free gas mole is used as an indicator for the hydrate formation rate. If the Cartesian plot of free gas mole versus time shows an exponential behavior it is an indication of a first order reaction. If the same data is plotted as natural logarithm of free gas mole versus time, the resulting line should fit a straight line. **Figure 4** gives the Cartesian plot of the experimental data for the test with pure-water (T-1). As observed, it exhibits an exponential behavior from which a first order reaction can be assumed.

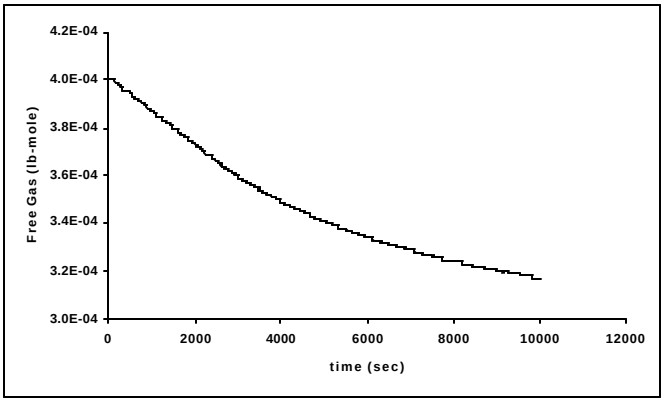

Figure 4. Cartesian plot of free gas versus time for the test with pure water (T-1)

A first order reaction equation is defined with the following expression;

$$N = N_0 e^{-kt} \qquad \text{(Equation-1)}$$

Where, N: Total number of moles at any time t; N_0: Initial number of moles; k: Rate constant, sec^{-1}; t: Time, sec.

When the natural logarithm of above equation is taken, the slope of ln(N) versus time graph is equal to rate constant k. When the derivative of the N with respect to time is taken, it will give the decrease in free gas content rate and it is relative to the hydrate formation rate so after that point it is going to be called hydrate formation rate.

$$\frac{dN}{dt} = -N_0 k e^{-kt} \qquad \text{(Equation-2)}$$

Thus, hydrate formation rate can be calculated at a specified time by Equation 2. First 30 minutes data of all experiments after the start of rocking are used to estimate the rate constants and hydrate formation rates.

Semi-logarithmic plot of the same data of Figure 4 is presented in **Figure 5** showing a linear behavior. Its best fit as a straight line has a correlation coefficient very close to unity. The slope of the straight line, 3.653E-05 for this case, is the rate constant with a unit of sec^{-1}. The rate constants and hydrate formation rates for all of the PVP and PEO experiments were determined and they are tabulated in **Table 2** and **Table 3**, respectively.

Table 2. Methane Hydrate Formation Rates with PVP Solutions

PVP (weight %)	k (sec^{-1})	Rate (lb-mole/sec)
0.000	3.653E-5	1.37E-8
0.010	3.540E-6	1.37E-9
0.100	4.735E-6	1.83E-9
0.500	2.457E-6	9.54E-10
1.000	2.398E-6	9.65E-10

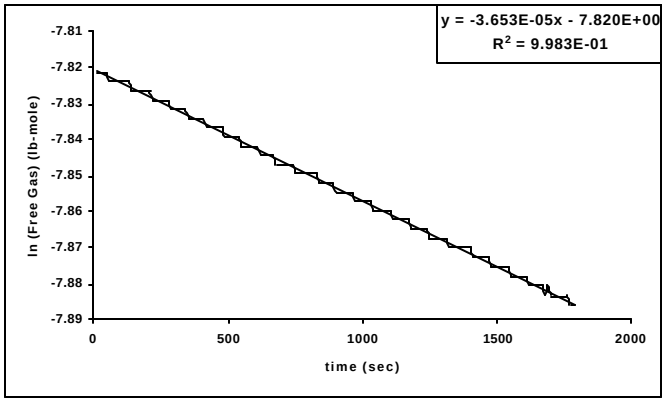

Figure 5. Semi-logarithmic plot of free gas versus time for the test with pure water (T-1)

Table 3. Methane Hydrate Formation Rates with PEO Solutions

PEO (weight %)	k (sec^{-1})	Rate (lb-mole/sec)
0.000	3.65E-5	1.37E-8
0.010	5.94E-6	2.35E-9
0.025	3.00E-6	1.19E-9
0.050	1.90E-6	7.58E-10
0.100	2.39E-6	9.52E-10
1.000	2.83E-6	1.12E-9

Hydrate formation rates in tables are in ascending order. As it is seen, for all of the concentrations of PVP and PEO formation rates are less than that of pure water. **Figure 6** and **Figure 7** present the hydrate formation rates in graphical form. As seen from Figure 6 and 7, the lowest methane hydrate formation rate (calculated from first 30 minutes of data) is about 14 times for PVP and about 18 times for PEO less than pure water experiment. Those results show that PEO is a good candidate of hydrate inhibitor.

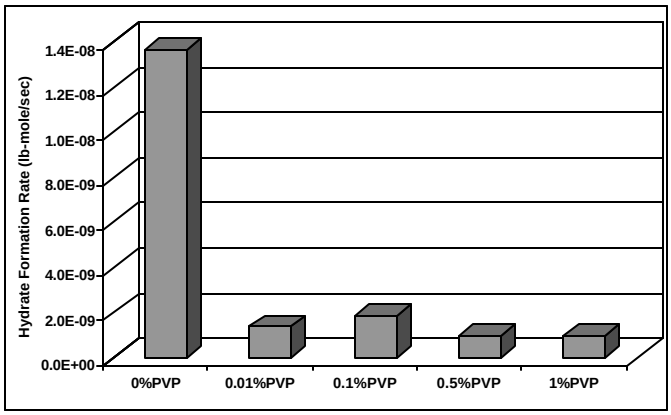

Figure 6. Methane hydrate formation rate with 0, 0.01, 0.1, 0.5 and 1 weight % PVP solutions.

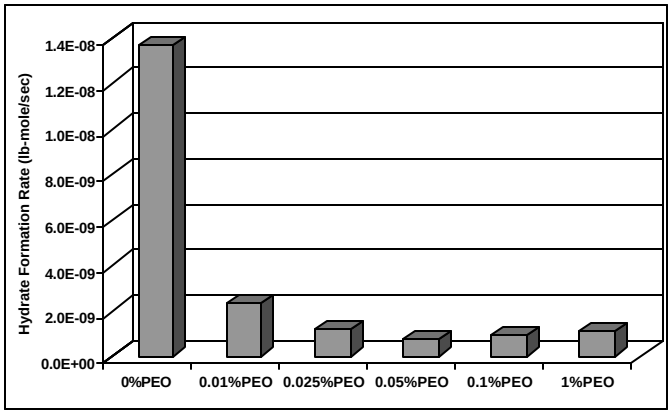

Figure 7. Methane hydrate formation rate within 0, 0.01, 0.025, 0.05, 0.1 and 1% PEO solutions

Conclusions

The following conclusions can be drawn from the analysis of experimental data of this study.

A known, patented hydrate inhibitor, PVP, was used to test the performance of experimental set-up and procedure of this study. The results showed that PVP is a good methane hydrate inhibitor and the experimental set-up and procedure are suitable for testing hydrate inhibition analysis.

PEO exhibits hydrate inhibition characteristics as a concentration of as low as 0.1 weight % and has not been known as a hydrate inhibitor until this study. This study shows that PEO prevents the methane hydrate formation within the first 60 minutes period from the start of rocking. After that period of time hydrate formation rate is still very low with respect to experiment carried out with pure water and methane gas. As a result, PEO is a good candidate of methane hydrate formation.

Since PVP is labelled as carciogenic, PEO can be a better candidate for hydrate inhibition in terms of health and safety considerations.

Acknowledgment. The authors wish to express their thankfulness to The Scientific and Technical Research Council of Turkey (TÜBITAK) for the financial support of this work.

References

(1) Sloan E.D., Jr. *Energy and Fuels*, **1998**, *12*, pp. 191-196.
(2) Kelland M.A.; Svartaas T.M.;and Dybvik L. *SPE 30695, Proceedings of the SPE Annual Technical Conference*, **1995**, pp. 529-537.
(3) Phillips N.J. and Kelland M.A. *Industrial Applications of Surfactants IV*; Karsa D.R., Royal Society of Chemistry, **1999**, pp. 244-259.
(4) Freer E.M. and Sloan E.D. *Ann. N.Y. Acad. Sci.*, **2000**, *912*, pp. 651-657.
(5) Karaaslan U. *Ph.D. Thesis*, Middle East Technical University, Ankara, 2001.

KINETICS OF CO_2 HYDRATE FORMATION BELOW MELTING POINT OF ICE

Takeshi Komai, Taro Kawamura, and Yoshitaka Yamamoto

National Institute for Advanced industrial
Science and Technology
16-1 Onogawa, Tsukuba
305-8569 Japan

Introduction

Gas hydrates are very attractive from both resources and environmental aspects. CO_2 gas hydrate can be utilized to develop methane gas hydrate as an important energy source in the near future. When producing methane gas from gas hydrate reservoirs at permafrost area, the injection of CO_2 might be used to promote the gas production by replacement, and to maintain the stability of strata due to the formation of CO_2 gas hydrate. In addition, the sequestration of CO_2 mass can be performed in the process of gas hydrate production. An experiment on the formation of CO_2 gas hydrates was carried out under low temperature below melting point of ice, using a specially designed cell-type apparatus. To observe the nucleation and formation process, CO_2 gas was introduced to the ice crystals in a pressure cell at a condition of high pressure. Raman spectrometry was used to measure the rate of formation based on Raman analysis due to the dynamic behavior of guest molecules. As a result, it was found that the rate of formation of CO_2 gas hydrate depends on various conditions, such as temperature, pressure and diameter of ice crystals. The mechanism of the formation of CO_2 gas hydrate under low temperature was also discussed, based on the results of Raman analysis.

Experimental

Apparatus. The experimental apparatus was specially designed and equipped for the formation and replacement of gas hydrates. It can be used under the various conditions that pressure, temperature and concentration of gases are precisely controlled. **Fig.1** illustrates the schematic diagram of the apparatus and measuring system used in the experiment. The pressure cell, made of stainless steel with a 3.2 ml internal volume, can be used at a pressure condition of up to 20 MPa. It contains a glass window for observing Raman scattering of monochromatic lights, a thermoelectric temperature control module, and some nozzles for the introduction of gas and liquid components. The pressure cell is installed on a constant temperature plate filled with a cooling agent methanol, where the temperature can be controlled with an accuracy of ±0.1 K. It is equipped with transducers for detecting and controlling pressures with an accuracy of ±0.05 MPa.

Measuring Methods. The observation system of the Raman spectroscopy and a CCD camera are mounted in the apparatus. The mechanism and theoretical background of Raman analysis are described in **Fig.2**. The figure also shows the molecular model of CO_2 gas hydrate. Macro mode is applied for the measurement of Raman spectroscopy, in which Ar laser is emitted to the sample. In this experiment powder-like fine ice crystals were placed in the pressure cell for the starter of gas hydrate. The average diameter of the crystals is about 9 micro meters. CO_2 gas was introduced into the cell and the pressure was controlled to a value of a little higher than the equilibrium pressure. During the nucleation and crystal growth of CO_2 gas hydrate, Raman spectra were measured and analyzed to get the data of Raman shifts. As the strength of Raman shift is proportional to the concentration of guest component, the formation rate can be calculated by the relative strength. In this experiment temperature condition was changed to the range between –18.5 deg. C. and 0 deg. C.. The pressure condition in the formation process of gas hydrate was set to a constant value of 1.6 MPa.

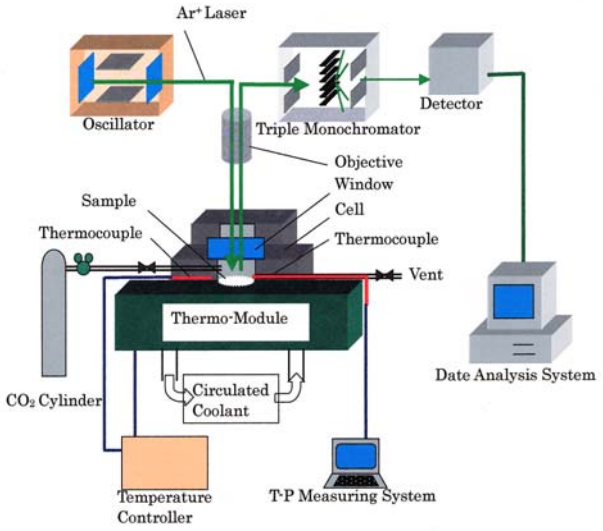

Fig.1 Experimental apparatus and measuring system of Raman spectroscopy.

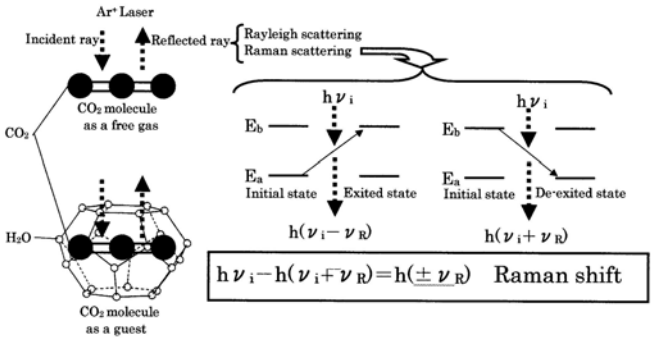

Fig. 2 Molecular model of CO_2 gas hydrate and the mechanism of Raman measurement.

Results and Discussion

In-situ measurement of formation process. As a typical result of measurement, **Fig.3** shows the trend of Raman shifts observed in the formation of CO_2 gas hydrate under a condition of –8.7 deg. C. and 1.6 MPa. Four peaks of Raman shift appeared as a result of Raman analysis in the process of guest molecule trap into the cages. The left hand peaks reveal the existence of CO_2 in large cage. It was found that the strength of the peaks gradually increased with time, and especially the rate of increase was quite large in the first stage of the formation, such as within 10 minutes. In this duration the formation mechanism is nucleation or transformation from ice to gas hydrate.

Formation rate of CO_2 hydrate vs Temperature. The comparison of time growth of the strength was made for the formation of CO_2 gas hydrate under the temperature condition that was changed between –18.5 deg C. and 0.5 deg. C.. **Fig.4** shows the relative strength of Raman shifts, in which the effect of temperature on the formation rate of CO_2 gas hydrate from ice crystals was described. From the result it was found that the rate of formation was very large in a condition of -0.5 deg C., compared with other conditions below –3.8 deg. C..

The result suggests that the nucleation phenomena or mechanism of CO_2 gas hydrate formation dramatically changes around the melting point of ice. This kind of effect is very much singular because in a normal situation the formation rate might increase as the temperature becomes lower. It is considered that the effect is caused by the existence of quasi-liquid layer at the interface of gas and hydrate sample. The liquid-like layer might accelerate the nucleation of gas hydrate and the rate of formation has a close relation with the thickness of the layer.

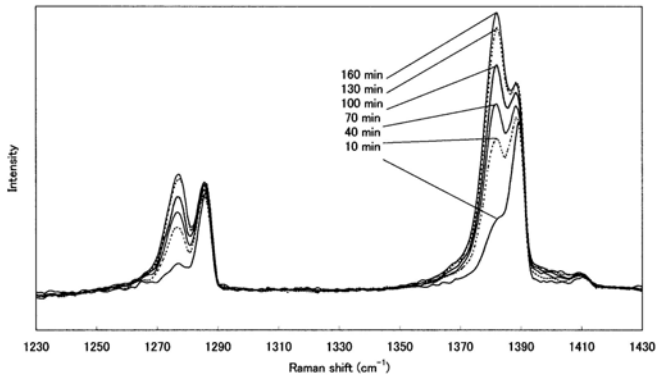

Fig.3 Raman spectra of CO2 gas hydrate obtained every 30 minutes.

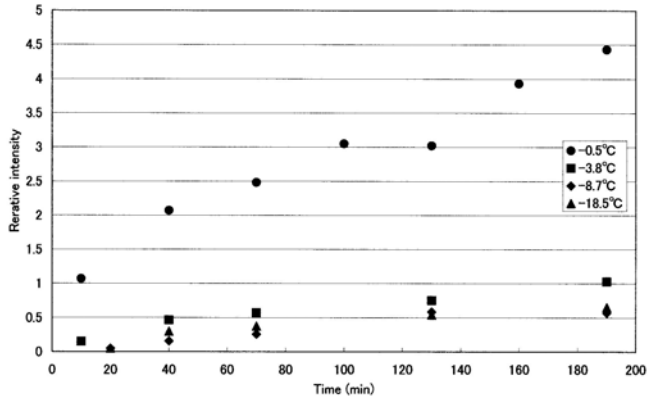

Fig.4 Time growth of relative strength obtained by Raman analysis as a parameter of temperature.

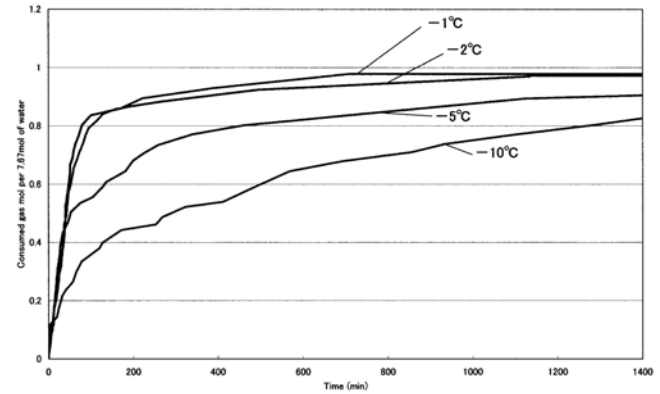

Fig.5 The formation rate of CO_2 gas hydrate obtained in bulk-scale experiment as a parameter of temperature.

Growth rate by bulk-scale experiment. The bulk-scale experiment for the formation of CO_2 hydrate was conducted using a pressure vessel with a volume of 200 mL. The rate of formation was obtained to measure the consumption of CO_2 in the process of transformation into gas hydrate. **Fig.5** illustrates the time growth of CO_2 gas hydrate for the bulk-scale experiment. The vertical axis means the consumed gas mole per mole of water. It is clear that the process of formation divides into two stages, especially in the case of temperature around meting point of ice. In other words, the formation of gas hydrate is very fast in the first stage of time growth within 200 minutes. However, the rate of formation became slower in the second stage of time growth. The result of this experiment agrees well with the result of Raman analysis, so that the rate of formation shows the maximum under a temperature condition between –1 to –2 deg. C.

The mechanism of time growth. Based on the results of Raman analysis and bulk-scale experiment, the mechanism of crystal growth and the resulted rate of formation of CO_2 gas hydrate can be qualitatively discussed. The most important factor in the first stage is considered to be the existence of liquid-like layer around the nucleation area. The thickness of the layer depends on the condition of temperature and ice surface. It makes sense to explain the effect of temperature on the formation rate of gas hydrate. On the contrary, the controlled factor might be the diffusion coefficient of gas between ice and hydrate, because the rate of formation became slower with time due to the blocking of gas transport through media. By the quantitative evaluation using a mathematical model, the rate of formation can be calculated as factors of temperature, pressure and other parameters. These kinetic data and the mechanism of crystal growth are very important to evaluate the formation behaviors of CO_2 gas hydrate under the real environment, such as marine sediments and permafrost.

Conclusions

The direct measurement by Raman spectroscopy is very effective to obtain kinetic data of gas hydrate formation. The rates of CO_2 gas hydrate formation were measured by Raman analysis and bulk-scale experiment as a fuction of temperature. The result showed that the effect of temperature on the gas hydrate formation was nonlinear and singular. It is suggested that the effect is due to the kinetic behavior of ice crystal and gas hydrate. The rate of CO_2 gas hydrate formation can be estimated to develop the kinetic model of ice and hydrate. More scientific research is needed to make clear the phenonenon.

Acknowledgment

We acknowledge Dr. S. P. Kang to conduct the measurement of Raman spectroscopy in this work, and thank Dr. K. Nagashima to carry out the data analysis of Raman spectra.

References

1. Furukawa, Y.,Yamamoto, M., Kuroda, T., J. Crystal Growth, 82, p.655, (1987)
2. Takeya, S., Hondo, T., Uchida, T., Ann. New York Academy Sci., 912, p.973, (2000)
3. Ikeda, T., Mae, S., Uchida, T., Chem. Phys., 108, p.1352, (1998)
4. Komai, T., Yamamoto, Y., Ohga, K., Ann. New York academy Sci., 912, 272, (2000)
5. Nakano, S., Moritoki, M., Ohgaki, K., J. Chem. Eng. Data, 43, p.807, (1998)

Corresponding author: Dr. Takeshi Komai, Thsukuba-West, AIST, 16-1 Onogawa, Tsukuba, 305-8569 Japan <koma@ni.aist.go.jp>

METHANE STORAGE IN HYDRATE FORM USING CALCIUM HYPOCHLORITE AS ADDITIVE

Shuan-Shi Fan, Yan-Kun Guo, Kai-Hua Guo, Yong Chen

Guangzhou Institute of Energy Conversion, The Chinese Academy of Sciences, 81 Center Martyr's Road, Guangzhou 510070, China

Introduction

Natural gas storage is a subject of great interest to many industries and particularly for transportation. Compressed natural gas, liquefied natural gas and adsorbent natural gas are widely techniques used. The possibility of developing a convenient storage system based on hydrate has been explored for about ten years around the world [1-6]. Gudmundsson[2] has focused on the storage and transportation of gas as hydrate at atmospheric pressure since 1990. Khokhar[3] used 1,3-dimethylcyclohexane and polyvinylpyrrolidone as additives to lower hydrate formation pressure. Also, Saito[4] used tetrahydrofuran or acetone, Rogers [5] used sodium dodecyl sulfate as accelerator to natural gas hydrates formation respectively. In this work, the effects of calcium hypochlorite on hydrate formation are investigated. The data shows that it can lower the degree of supercooling and enhance the relative cage occupancies.

Experimental

The schematic diagram of the apparatus is shown in Fig.1. The cell is cylindrical, immersed in a constant temperature water bath. Its inside diameter is 2.5cm, and the length is 4.5 cm, with a total volume of 24.3cc. A constant pressure regulator is equipped. The temperature of the cell was monitored with a platinum resistance probe accurate to ±0.1℃, and pressure was monitored via a 6.0Mpa gauge accurate to 0.4% of full scale. An electronic balance accurate to ±0.01g was used to detect the mass increment of the cell through the experiment.

The methane was produced by Guangzhou Gas Factory, with a purity of 99.9%. Doubly re-distilled water was used. The calcium hypochlorite was pure grade, purchased from Shanghai Fouth Reagent Factory.

All the experiments were carried out under 4.0MPa at 273.3K. Water, weights m_w, and 1% (mass fraction) of calcium hypochlorite was loaded into the cell as condensed phase. Vacuum the system and weight the cell's mass, expressed as m_1. After the system was refrigerated to 273.3K, charge methane in. Then weight the cell every 3 hours until the mass, expressed as m_2, does not change perceptible. The mass increments, $\Delta m=m_2-m_1$, in a series of experiments are listed in Table 1.

For compare, data for water/methane binary system under the referred pressure and temperature were tested also.

1. Results

2.1 data processing[6]

To calculate the storage capacity expressed as volume gas/volume hydrate (Vol/Vol) from the experimental data, trail and error procedures were applied.

For ideal structure I hydrates, if all of the cavities were filled, the hydration number (water molecules per guest molecular) would be n =46/8. For methane, which formed structure I hydrate, the hydration number is related to the fractional filling of the large and small cavities, y_L and y_s, respectively as:

$$n=\frac{46}{6y_L+2y_s} \tag{1}$$

And for a simple hydrate at 273.15K, y_L and y_s interrelates as:

$$-0.4885=\frac{3}{23}\ln(1-y_L)+\frac{1}{23}\ln(1-y_s) \tag{2}$$

The methane hydrate density(ρ) may be calculated by the formula:

$$\rho=\frac{\frac{N_w}{N_{Ava}}\left[M_{H2O}+\left(y_L\upsilon_L+y_s\upsilon_S\right)M_{CH4}\right]}{V_{Cell}} \tag{3}$$

where, N_w is the number of water molecules per unit cell; N_{Ava}, Avagadro's number, 6.023×10^{23} molecules/mol; $M_{H2O,CH4}$, molecular weight of H_2O and CH_4;y_L, y_s, fractional occupation of large/small cavity by CH_4; ν_L, ν_s, number of large/small cavities per water molecule in unit cell; V_{cell}, volume of unit cell.

A value of n may be estimated at 4.0MPa corresponding to 273.15K for CH_4. Equations (1) and (2) may then be solved simultaneously for y_L and y_s. Hydrate density can be calculated by Equation (3).

$$\Delta m=\Delta m_H+\Delta m_C \tag{4}$$

Where $\Delta m=m_2-m_1$, is measured mass increment; Δm_H, the mass of the methane trapped in hydrate; Δm_C, the mass of the methane over the hydrate as compressed gas.

Estimated a value of Δm_H, m_w and ρ are known quantity, the volume of hydrate can be calculated. Then Δm_C can be calculated by van der Waals equation, and get a new value of Δm_H. Use trail and error procedure to get the value of Δm_H corresponding to the hypothetical hydrate number.

Then the hydration number corresponding to Δm_H can be calculated. Substitute the calculated n value to Equations (1),(2),(3) to calculate the density of the hydrate, Δm_H, until a new n. Go on the iteration utile the hydration number n is ultimately calculated. After n is calculated, Δm_H and Vol/Vol were calculated for each experiment.

2.2 Results

The experimental data and calculation results are listed in Table 1. Fig 2 describes the Vol/Vol value of a series of experiments. It is showed that m_w range from 3.73 to 16.51, correspond to about 15% to 68% of the cell volume. When m_w exceeds 8 grams, the Vol/Vol value tends to reduce slightly with the increasing of m_w. It shows that the formation reaction was mass-transfer limited. As shown in figure 2, the Vol/Vol value varies from 134 to 176. Averagely, 151 volumes of methane (standard pressure and temperature) were trapped in one volume hydrate. Calcium hypochlorite has two evident effects on methane hydrate formation. Firstly, it reduces the degree of supercooling. In these experiments for water/methane binary system, no hydrates were observed in 20 hours under the mentioned temperature. After calcium hypoclorite is introduced, typically the formation begin in 6 hours, but it seems to be stochastic. Secondly, calcium hypochlorite helps most of the water

molecules to form hydrates in a relatively short time under moderate conditions. For different experiments, hydration number lies between 6.11 and 8.32. Its average magnitude is 7.36, indicating 78% of the large and small cavities in the lattices were occupied by methane molecules. The satisfactory effect of this compound makes the stabilization and transportation of natural gas as hydrates more feasible.

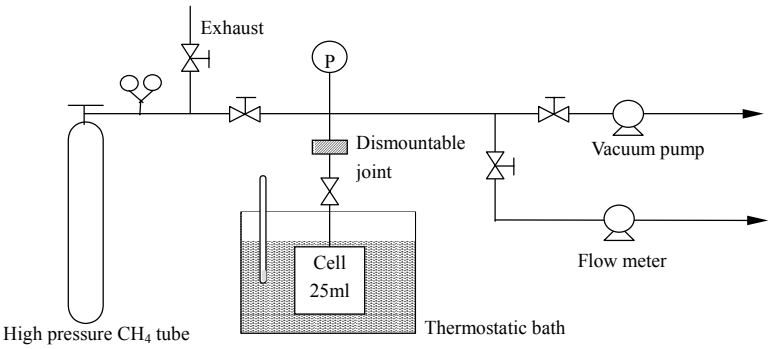

Fig 1. Schematic diagram of the experimental apparatus

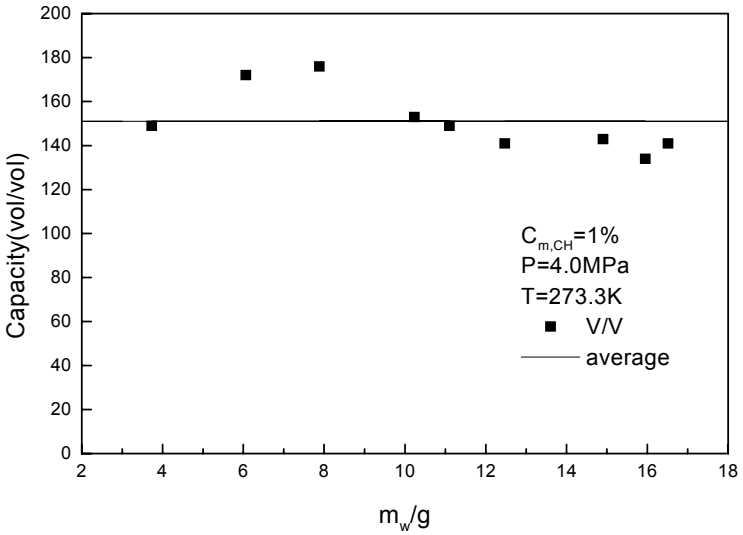

Fig. 2. Volume gas(standard conditions)/volume hydrate in a series of experiments

Table 1. Summary of experimental data and results

m_w	Δ m	Δm_H	Vol/Vol	Hydration Number
3.73	1.07	0.45	149	7.40
6.06	1.38	0.85	172	6.32
7.88	1.6	1.14	176	6.11
10.23	1.64	1.27	153	7.15
11.1	1.67	1.33	149	7.40
12.47	1.69	1.4	141	7.90
14.9	1.9	1.71	143	7.75
15.95	1.86	1.7	134	8.32
16.51	2	1.87	141	7.85

Conclusion

The potential of methane storage in hydrate form with calcium hypochlorite as additive was investigated. Calcium hypochlorite reduced the degree of supercooling on methane hydrate formation. It also helped most of the water molecules to form hydrates in a relatively short time under moderate conditions.

The formed gas hydrates had the ability to store 134 to 176 volumes of methane per volume of hydrate, averagely, 151, at 273.3K and 4.0MPa. The hydration numbers of which were between 6.11 and 8.32.

References

(1). 2001. Peking. Century Petroleum Forum.

(2). Gudmundsson J S, et al, In: AIChE Spring National Meeting, New Orleans, March(1992)

(3). Khokhar A A, et al, Fluid Phase Equilibria 150-151(1998):383

(4). Saito Y, et al, In: 2nd International conference on natural gas hydrates, Toulouse France, June2-6,1996

(5). Rogers R E, et al, In: 3rd International conference on natural gas hydrates, Salt Lake City, Utah, USA, July, 18-29, 1999

(6). Sloan E D, Clathrate Hydrate of Natural Gases, 2nd edn., Marcel Dekker, New York, 1998

PHYSICAL PROPERTIES AND CONVERSION OF METHANE HYDRATES

Dirk D. Link, Edward P. Ladner, Heather A. Elsen, and Charles E. Taylor

U.S. Department of Energy
National Energy Technology Laboratory
P.O. Box 10940
Pittsburgh, PA 15236-0940

Introduction

Methane hydrates were first observed in the laboratory in 1810. It wasn't until nearly 150 years later that they were observed in nature. Hydrates can occur in permafrost, in sediment where gas exists under moderate to high pressure and low temperatures, and offshore beneath deep water. Hydrates are a problem in the oil and gas production industry because they can form in the well or pipelines, thereby blocking the flow of fuel. Estimates by the U.S. Geological Survey project that world hydrate deposits contain approximately 2 x 10^4 trillion cubic meters of methane [1]. Estimates of methane hydrate deposits off the coast of the United States is approximately 9 x 10^3 trillion cubic meters of methane with an additional 17 trillion cubic meters of methane in the permafrost on the north slope of Alaska [1].

Recent publications have indicated that photochemical oxidation of methane may be a commercially feasible route to methanol [2,3]. Previous research in our laboratory [4] has shown that, methane, dissolved in water, at temperatures > 70 °C, with a semiconductor catalyst, can be converted to methanol and hydrogen. The limiting factor for conversion of methane appears to be the solubility of methane in water. We hypothesized that if the concentration of methane in water can be increased, conversion should also increase. Methane hydrates might provide a method of increasing the amount of methane dissolved in water, because at standard temperature and pressure (STP), one volume of saturated methane hydrates contains approximately 180 volumes of methane.

Our vision is to immobilize methane and water in close proximity by formation of the methane hydrate. The reaction will involve the formation of hydroxyl radical (•OH) within the methane hydrate by photochemical means. The proximity and restricted mobility of the •OH and the CH_4 would then favor the formation of CH_3OH. Successful demonstration of this principle would then open the possibility of using hydrates to immobilize reactants in a way that favors the desired selectivity. This is the basis of our Patent [5].

EXPERIMENTAL

All reactions were conducted in a high-pressure view cell. The cell is constructed of 316 stainless steel 6.35 cm (2.5 inches) OD and 27.4 cm (11 inches) in length. The internal volume of the cell is ~ 40 mL. The cell is fitted with 2 machined endcaps, one which contains a sapphire window to allow for observation of the contents of the cell using a CCD camera. The cell is fitted with ports to accommodate the fill gas inlet and reaction product outlet, a pressure transducer to monitor the internal pressure of the gas inside the cell, and a thermocouple that terminates inside the cavity of the cell to monitor the temperature of the liquid/hydrate mixture. While the working pressure of the cell is rated at 220 MPa (32,000 psia), all experiments were conducted at 13.8 MPa (2000 psig) or less. The temperature of the cell is controlled by the flow of a glycol/water solution from an external circulating temperature bath through a coil of 0.64 cm (¼ inch) copper tubing that is wrapped around the outside of the cell. Several layers of insulating material are wrapped around the cell to help maintain constant temperature.

A typical experiment involves filling the cell with 40 mL of double-distilled water. A Teflon® coated stir bar is added, followed by portions of the photocatalyst. The endcap is placed on the cell and tightened to specifications. An external magnetic stirrer is used to obtain a high degree of vortex mixing inside the cell. The cell is connected to the gas manifold and purged several times with methane. Following the purge procedure, the cell is charged with methane at pressures of 5.5 – 13.8 MPa (800-2000 psig). Using the external circulating temperature bath, the temperature of the water in the cell is lowered until formation of the methane hydrate is observed. After formation of the hydrate, the temperature of the cell is lowered to -5 °C and held constant. Illumination of the hydrate is then performed using a high-pressure 350-watt mercury-vapor lamp, with the light directed toward the sapphire window. After illumination for a set period of time, the cell is allowed to warm slowly to room temperature. When the cell and its contents have reached room temperature, the contents of the cell are vented and a gas chromatograph and/or a mass spectrometer are used to analyze the products.

Multiple hydrate formation experiments were conducted using the following solutions: 30 mL of double distilled water, 30 mL of simulated seawater (made by by dissolving 26.8 grams of sodium chloride and 5.3 grams of magnesium chloride in 1 liter of double-distilled water), or water with surfactant (added at a concentration of 224 ppm). The cell was connected to the reactor manifold and charged with methane as described above. The temperature of the cell was reduced to 5°C and held constant until the methane hydrate formed. After formation of the methane hydrate, the cell's temperature was increased to 15°C. After the methane hydrate had dissociated, as observed through the cell's view port and the return of the cell pressure to that prior to hydrate formation, the temperature of the cell was reduced to 5°C. This procedure was repeated several times.

The experiments to determine maximum uptake of methane by the hydrate were conducted by filling the cell with 15 mL of double-distilled water and surfactant, adding the Teflon® coated stir bar, and sealing the cell, all as described above. The cell was connected to a modified gas manifold containing two single-stage high-pressure regulators in series and purged several times with methane. However, after the last purge, the valves connecting the cell to the manifold were not closed at this point. Rather, the regulators were set to deliver methane at 9.7 MPa (1400 psig), in order to allow the experiment to proceed at a constant head pressure of 9.7 MPa (1400 psig) during the formation of the hydrate. Again, an external magnetic stirrer was used to obtain a high degree of vortex mixing inside the cell. Temperature of the water in the cell was lowered until formation of the methane hydrate is observed. Following formation of the hydrate, the temperature of the cell is lowered to -5 °C to minimize the dissociation of the hydrate in the subsequent depressurization step. After 8 hours at -5 °C, the cell is isolated from the manifold and the head pressure released. After release of the head pressure, the cell was re-sealed and warmed to room temperature.

RESULTS

Our first experiments were to study the formation and dissociation of methane hydrates. Figure 1 shows a typical pressure/temperature profile for this process. During the initial stages of cooling, the pressure inside the cell mirrors that which would be predicted from the ideal gas law. However, as the hydrate begins to form, a sharp decrease in the cell pressure is observed, indicating that methane is being absorbed from the headspace. Visually, the initial

hydrate formation appears as ice crystals suspended in the water. As formation of the hydrate continues, the hydrate begins to agglomerate, forming a slush. Within a few seconds, the slush is transformed into a solid mass.

Figure 1. Pressure and temperature profile as a function of time for the formation of a methane hydrate from double distilled water.

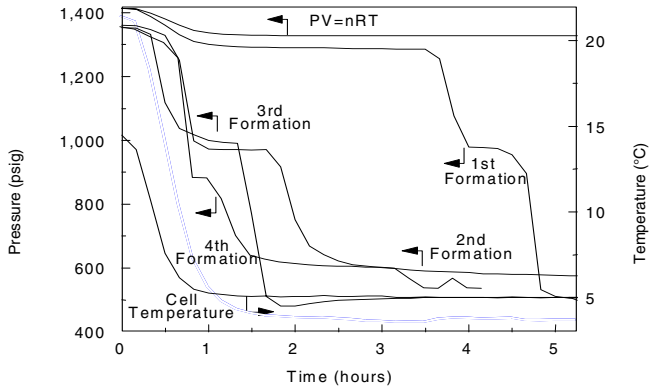

Even after formation of the solid mass, over time the hydrate incorporates more of the free methane into the crystal structure. This is evident by a decrease in the pressure in the cell over time as shown in Figure 1. Upon warming, the hydrate dissociates with evolution of methane from the slush. After dissociation of the hydrate, subsequently decreasing the temperature can reform the methane hydrate. This is also shown in **Figure 1.** Note that the hydrate forms notably faster during the second formation (1 hour as opposed to 4 hours). The third and forth formation of the hydrate occur at times slightly less than the second formation. This decrease in formation time may be due to microscopic hydrate crystals that are still present in the solution, even at 15 °C. These crystals would act as seeds for future formations. The formation of methane hydrates in water that contains the suspended photocatalyst followed the same physical changes as that observed for hydrate formed in pure water.

Formation of methane hydrates in double-distilled water, simulated sea water and double-distilled with a surfactant added is shown in Figure 2. As is shown in the figure, methane uptake by both double-distilled and simulated seawater is ~1.4 MPa (200 psig). Also of note is that the onset of hydrate formation in the simulated seawater is 3°C lower than that of the double-distilled water. When surfactant is adder to the water, methane uptake by the hydrate is ~5.6 MPa (800 psig), a four-fold increase. The increase observed in the uptake of methane when the surfactant is present can be explained what happens when hydrates form. Since methane hydrate is less dense than water, hydrates form on the surface of the water. Even with stirring, soon enough hydrate is present that the entire surface of the water is covered by the hydrate. This prevents additional methane from dissolving in the water. When the surfactant is present, the hydrate formed is forced to the edges of the surface, allowing the water-methane contact to be present longer, allowing the concentration of methane in the water to remain constant throughout formation.

In order to determine the maximum amount of methane that we could have taken up by the hydrate, we formed methane hydrate in double-distilled water containing 224-ppm surfactant under a constant head pressure of 9.7 MPa (1400 psig). The results are shown in Figure 3. During this experiment, the hydrate was formed under a constant head pressure of 1400 psig, with formation beginning at approximately 3.5 °C. The temperature of the cell was further decreased to -5 °C, in order to preserve the hydrate during the subsequent depressurization of the cell. Following depressurization at -5 °C, the cell was armed to room temperature, accompanied by an increase in cell pressure due to methane outgassing from the melting hydrate. As Figure 3 shows, the cell pressure reached approximately 1350 psig. The hydrate formed by this method contained over 96% of the maximum theoretical amount of methane.

Figure 2. Pressure as a function of temperature for the formation of a methane hydrate in double-distilled water, simulated seawater, and water with 224-ppm surfactant added.

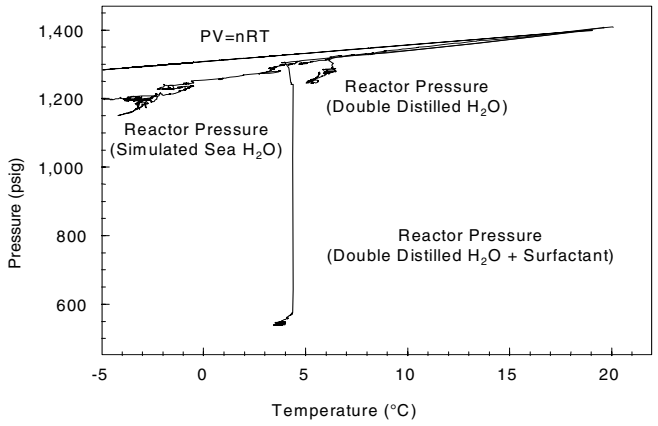

After the hydrate had formed and the pressure in the cell equilibrated, the UV lamp was turned on to initiate the photocatalytic conversion process. During illumination, a decrease in the pressure of the cell is observed. Following illumination, the cell was maintained at -2 °C for several hours before warming to room temperature. Also of note is that the final pressure of methane is less than the starting methane pressure due to conversion of the methane within the hydrate.

Figure 3. Pressure and temperature profile as a function of time for the formation of a methane hydrate with 224 ppm surfactant added.

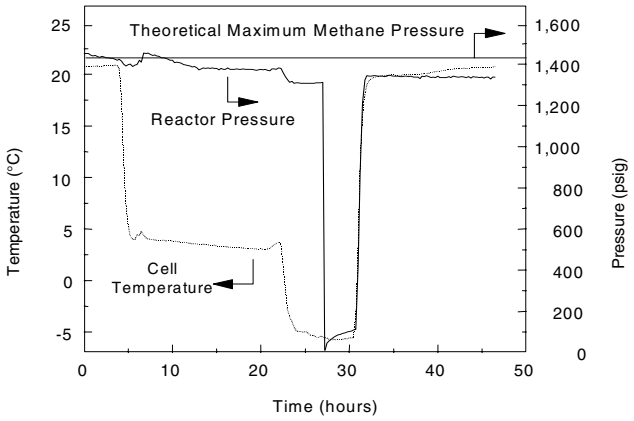

Mass spectrometric analysis of the gas vented from the cell after illumination revealed the presence of methanol, hydrogen, ethane, oxygen, formic acid, and carbon dioxide, as shown in Figure 4. Side reactions that occur during the photocatalytic conversion process are responsible for producing these additional species. Photocatalytic

splitting of water forms oxygen, ethane is formed by the combination of two methyl radicals, and the formic acid and carbon dioxide are the result of further reactions of methanol.

Attempts to use GC to identify products dissolved in the water after reaction were of limited value. In an effort to detect these products dissolved in the water, the cell and its contents were heated to 70°C prior to venting. Analysis of the gas headspace resulted in the detection of similar products as those obtained at room temperature. If products dissolved in the water were present, their concentration was too low to be detected with our setup. We are currently refining our detection system to correct this problem.

Figure 4. Product analysis for the photoconversion of methane hydrate.

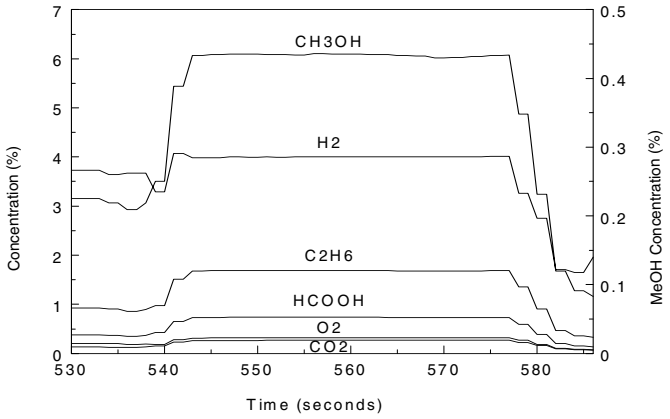

Experiments were also performed where the double-distilled water was replaced with simulated seawater. The results of these experiments were similar to those performed with double-distilled water.

CONCLUSIONS

We have produced methane hydrates in our laboratory. The temperature and pressure profiles for hydrate formation for several different starting pressures of methane, as well as different aqueous media, have been determined. Using a photocatalytic process, we have been able to convert the methane hydrate to methanol and hydrogen. We also observe several side reactions of methane hydrates, producing ethane, oxygen, formic acid and carbon dioxide.

Previous research [4] in our laboratory had shown that the photocatalytic reaction of methane and water did not occur below 70°C. However, current studies have demonstrated effective conversion of methane hydrates using the same catalyst at temperatures below 0°C [5].

The addition of a surfactant improves the uptake of methane during formation of the hydrate. The amount of methane uptake obtained using the surfactant has reached greater than 96% of the theoretical limit.

This process, while still in its infancy, may provide a method for recovering the methane contained within hydrate deposits. In addition, it may provide an effective method for removing hydrate plugs from pipelines and wells.

DISCLAIMER

Reference in this report to any specific commercial product, process, or service is to facilitate understanding and does not necessarily imply its endorsement or favoring by the United States Department of Energy.

ACKNOWLEDGEMENTS

The authors would like to acknowledge the technical assistance of Jennifer Bennett.

REFERENCES

(1) Collett, T.S. and Kuuskraa, V.A. *Oil and Gas J.* **May 11, 1998**, 90.
(2) Ashokkumar, M. and Maruthamuthu, P. *J. Mat. Sci. Le*tt.**1988**, 24, 2135-39.
(3) Ogura, K. and Kataoka, M. *J. Mol. Cat.* **1988**, 43, 371-79.
(4) Noceti, R.P. and Taylor, C.E. U.S. Patent 5,720,858 **February 24, 1998**.
(5) Taylor, C.E., Noceti, R.P., and Bockrath, B.C. U.S. Patent *6,267,849* **July 31, 2001**.

SIMULATIONS OF METHANE HYDRATE PHENOMENA OVER GEOLOGIC TIMESCALES: EFFECT OF MARINE BASIN PARAMETERS

Kevin L. Gering, PhD

Fossil Energy Technologies
Idaho National Engineering and Environmental Laboratory
P. O. Box 1625
Idaho Falls, ID 83415-3625

Introduction

The complex behavior tied to formation and accumulation of methane hydrate and free gas within dynamic marine sediments has been investigated using a new model that includes physical, mechanical, biological, and thermodynamic contributions. An early paper provided a detailed analysis of phase equilibria for the seawater-methane system within the context of having variable seafloor depths and geothermal gradients.[1] The paper that followed presented initial results of the newest model that incorporates accurate phase equilibria, sediment compaction, liquid advection, and methane biogenesis.[2] Rates of key processes are described in terms of geologic time, making possible simulations covering several million years.

This work extends our focus to look at the effects of marine basin parameters on the occurrence of solid methane hydrate and free gas. Foremost parameters include the geothermal gradient (GTG) and the depth of the seafloor, which are key to establishing the thermodynamic state of the seawater-methane system at a given sediment depth below the seafloor. Other basin parameters include the rate of sediment deposition and compaction, average pore diameters within the sediments, and the shape of sediment particles. Determination of conditions for maximum occurrence of methane hydrate is facilitated by a comprehensive study of these basin parameters. Hence, resource determination is made possible by this model, whereas other applications could include seafloor stability issues, and environmental release of methane from marine systems.

Methods

Sediment Dynamics. Marine sediments are porous media whose porosity profiles change over time due to a number of influences. Herein, the sediment compaction rate is defined as the change in sediment porosity over time as a function of sediment depth, where this rate dictates the downward migration of the sediment solids and the upward liquid advection rate. This work developed an analytical expression for porosity as a function of depth and time that is essentially a time-modified version of the well-accepted Athy equation,[3] which has seen wide use in sedimentary geophysics because it can provide good estimates of porosity profiles for some marine basins.[4-7] Sediment compaction and liquid advection are heavily influenced by the physical characteristics of the sediment, and seawater advection due to compaction is the primary transport mechanism for moving methane to locations within the sediment where it can be formed into methane hydrate or free gas.

Key Basin Parameters. The depth of the seafloor and value of the GTG have profound effects on the amount of methane available from advecting liquid for hydrate formation or gas exsolution. Consider the idealized phase equilibria represented in **Figure 1**, wherein the phases are liquid seawater (L), methane hydrate (H), and free methane gas (G). If the GTG is assumed to be constant, then liquid advection pathways along a GTG are represented by straight lines on a depth versus temperature plot. Three such lines are shown in Fig. 1. Lines A and B represent the comparison of basins that have different seafloor depths, but have identical GTGs. Lines B and C represent the scenario of two basins that have the same seafloor depth, but differing GTGs. The potential magnitude and location of hydrate and free gas formations will vary between lines A, B, and C because the phase equilibria (as reflected by soluble methane concentrations) differs among these paths.

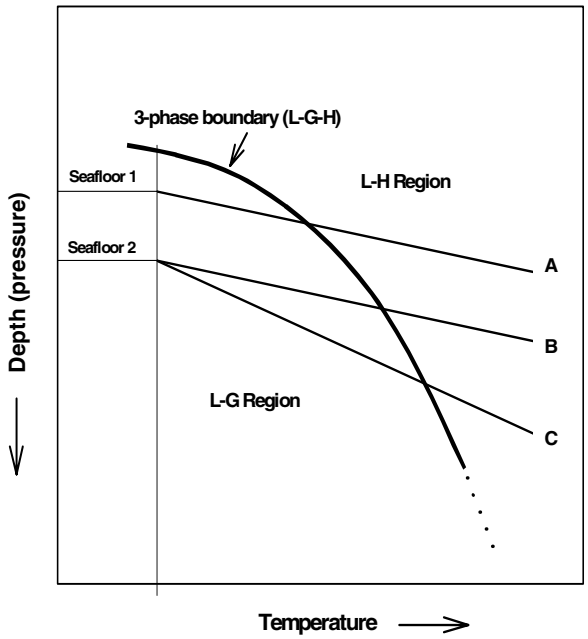

Figure 1. Idealized plot of phase equilibria for the seawater-methane system, contrasting the upward liquid advection paths taken along the same GTG with different seafloor depths (lines A and B) and different GTGs with the same seafloor depth (lines B and C).

Other parameters include rate of sediment deposition and compaction, average pore diameters between sediment particles, and the shape of sediment particles. Sediment deposition and compaction have a direct effect on the upward flux of advecting seawater, and hence influence the net migration of methane through the sediments over time. Pore sizes and particle shapes affect the frictional flow characteristics of the advecting liquid, and are key influences on liquid overpressures (those pressures experienced by advecting liquid that are greater than hydrostatic values).

Methane Biogenesis. A source term for biogenic methane has been incorporated into the model, which yields the production rate of methane as a function of depth and temperature. Predictions of methane generation within marine sediments are based on laboratory data gathered using isolated methanogens found in natural marine systems, assigning an average population of these microbes within the total microbial consortium. A previous paper should be consulted for further details concerning this biogenic source term.[2]

Results and Discussion

Methane within advecting liquid is considered available for hydrate or free gas formation if the advection path involves a change of thermodynamic states from higher to lower methane equilibrium concentrations. **Figure 2** shows the cumulative change of soluble (saturated) methane concentrations for seafloors at 500, 1000, and 2000m deep, and for GTGs of 20 and 40 °C per km. The inflection points represent crossing from the L-G region into the L-H region. It

is interesting to note that deeper seafloors actually cause methane to become subsaturated within advecting liquid until the three-phase boundary is reached, based solely on thermodynamic considerations. Shallower seafloors generally promote supersaturation of methane within seawater along the GTG-defined advection path. These observations lead to the assertions that bottom simulating reflectors (BSRs) would likely be absent for basins having deeper seafloors, since thermodynamic conditions along the GTG does not favor gas exsolution. Conversely, BSRs are more probable for shallower seafloors since it is thermodynamically feasible to produce free gas. All scenarios in Fig. 2 indicate that hydrate formation is possible for the advection paths within the L-H region, where more hydrate will be formed at higher GTG values.

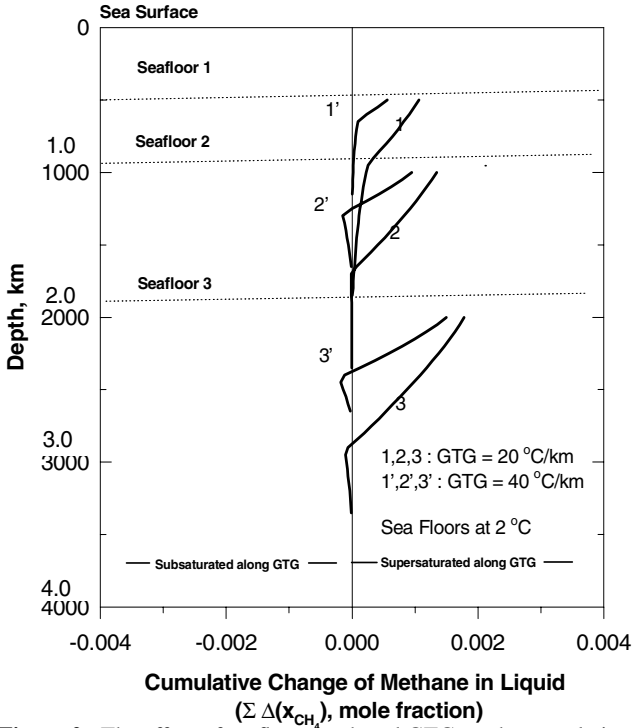

Figure 2. The effect of seafloor depth and GTG on the cumulative change of soluble methane in seawater along upward advection paths.

Up to this point considerations in Figs. 1 and 2 have been restricted to thermodynamic equilibrium conditions. However, it is necessary to superimpose phase equilibria upon a sediment compaction framework to quantify the amounts of soluble methane converted to hydrate and free gas over time. This was done for the case of having a constant seafloor depth, allowing simulations to run out to 20 Ma. **Figure 3** shows the velocity profiles for advecting liquid and settling sediment solids under conditions of a moderate sediment compaction rate. The fluid velocities are a key parameter in Darcian analyses of flow through the sediments, since they have a direct influence on liquid overpressures.

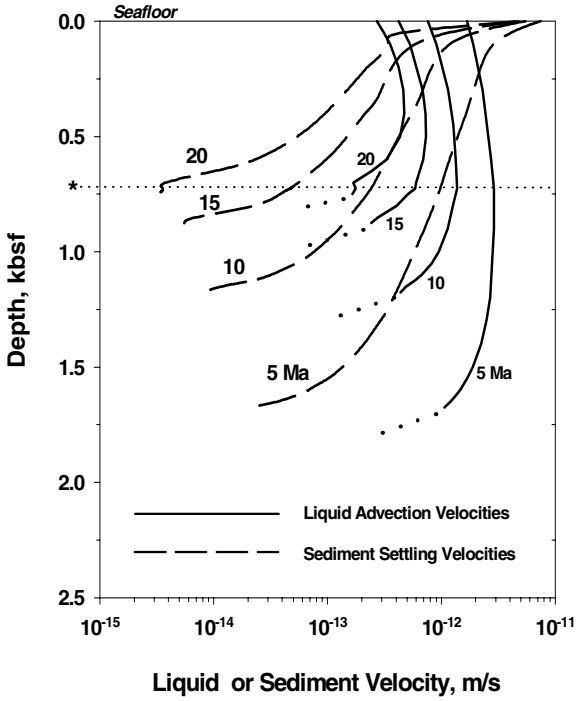

Figure 3. Velocity profiles of advecting liquid and sediment solids for the case of a "moderate" sediment compaction rate. The * represents the depth of greatest hydrate occurrence**.**

Figure 4 shows the net amounts of methane hydrate and free gas that have formed after 10 and 20 Ma, based on advection represented in Fig. 3. A GTG of 20 °C/km and a seafloor at 1000m were used in generating Fig. 4. It is seen in this figure that the greatest occurrences of hydrate and free gas lie within narrow bands of depth, which are generally located in the vicinity of where the advection path (GTG) crosses the three-phase boundary. Also shown is that the volume of free gas present at 10 Ma (5% by vol) disappears by 20 Ma. This disappearance is due to liquid overpressures that increase between 10 and 20 Ma as a consequence of lowered sediment porosity over time. These higher overpressures cause the local pressure experienced by the advecting liquid to shift from the L-G region into the L-H region, effectively enabling the free gas to be converted into hydrate. The amounts of hydrate shown in Fig. 4 are in good agreement with other investigators who have estimated hydrate occurrences in reasonably homogeneous sediments to fall between 1 and 12% by volume, depending on the age of the marine basin.[8-13]

Based on Fig. 2, we can speculate how the plots in Fig. 4 would change as the seafloor depth and GTG are changed. For example, shallower seafloors would yield shallower hydrate deposits with underlying free gas deposits. Deeper seafloors would correspond to deeper hydrate deposits that may be of a greater magnitude, with minimal free gas beneath. However, the shape and magnitude of the plots in Fig. 4 are also influenced by the sediment compaction rate. A faster compaction rate will yield somewhat different hydrate and free gas profiles (than a slower rate) because the higher liquid velocities will yield higher liquid overpressures that will cause a localized shift in phase equilibria conditions.

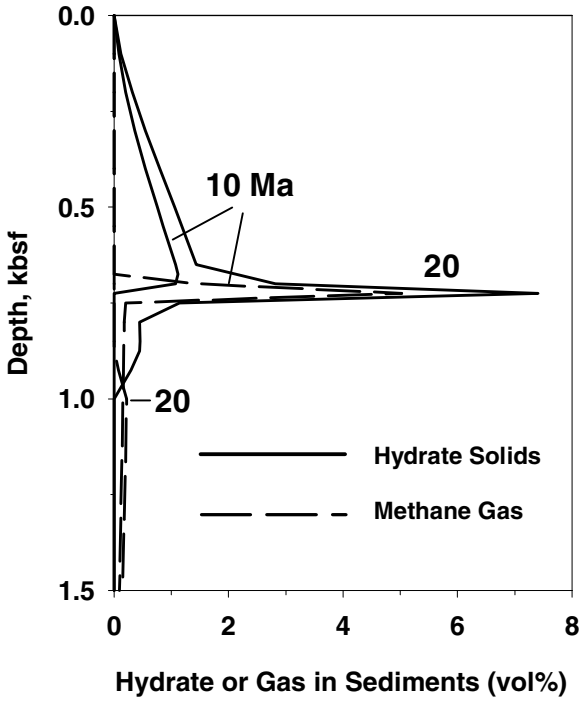

Figure 4. Predicted accumulation of methane hydrate and free gas within simulated compacting sediments undergoing a moderate compaction rate.

Conclusions

Occurrence of methane hydrate and exsolved methane gas within compacting marine sediments has been described by a advanced model incorporating accurate phase equilibria, sediment compaction, liquid advection, and methane biogenesis. Key parameters affecting the formation of hydrate and gas were discussed, which included the GTG and seafloor depth. Other parameters currently under investigation include the rate of sediment deposition and compaction, average pore diameters between sediment particles, and the shape of sediment particles. A large parameterized study can yield the optimal set of conditions for maximum hydrate and free gas formation. Results from a large-scale parameterized study will be given in the full presentation.

Acknowledgement. The author wishes to gratefully acknowledge that this work was funded by the United States Department of Energy under contract DE-AC07-99ID13727.

References

(1) Gering, K. L.; Cherry, R. S.; and Weinberg, D. M., *Ann. N.Y. Acad. Sci*., **2000**, *912,* 623.
(2) Gering, K. L., "Simulations of Methane Hydrate Phenomena over Geologic Timescales. Part I: Effect of Sediment Compaction Rates on Methane Hydrate and Free Gas Accumulations", submitted July 2001 to *Earth & Planetary Science Letters.*
(3) Athy, L. F., *Am. Assoc. Pet. Geol. Bull.*, **1930**, *14*, 1.
(4) Shi, Y.; and Wang, C., *J. Geophys. Res.,* **1986**, *91* (B2), 2153.
(5) Magara, K., *Soc. Pet. Eng. J*., **1971**, *2896*, 236.
(6) Hart, B. S.; Flemings, P. B.; and Deshpande, A., *Geology*, **1995**, *23* (1) 45.
(7) Yuan, T.; Spence, G. D.; and Hyndman, R. D., *J. Geophys. Res.*, **1994**, *99* (B3) 4413.
(8) Rempel, A. W.; and Buffett, B. A., *J. Geophys. Res*., **1997**, *102* (B5) 10,151.
(9) Rempel, A. W.; and Buffett, B. A., In *Gas Hydrates: Relevance to World Margin Stability and Climate Change*, J.-P. Henriet, J. Mienert, Eds.,Geological Society, London, Special Publications, **1998**, *137,* 63.
(10) Zatsepina, O. Ye.; and Buffett, B. A., *J. Geophys. Res*., **1998**, *103* (B10) 24,127.
(11) Buffett, B. A., *Annu. Rev. Earth Planet. Sci*., **2000**, *28,* 477.
(12) Davie, M. K.; and Buffett, B. A., *J. Geophys. Res.*, **2001**, *106* (B1) 497.
(13) Guerin, G.; Goldberg, D.; and Meltser, A., *J. Geophys. Res*., **1999**, *104* (B8) 17,781.